

# THREE-DIMENSIONAL MICRO-SITING OF OFFSHORE WIND FARMS

A three-dimensional micro-siting approach for efficient design of offshore wind farms, using CFD analysis in WindSim.

FRIDA VOLL HAREIDE

SUPERVISOR

Sathyajith Mathew

**University of Agder, 2024**

Faculty of Engineering and Science

Department of Engineering and Sciences



# Abstract

This master's thesis investigates a three-dimensional micro-siting approach for wind farms on the offshore wind site Southern Northsea II by wind farm simulation in the software WindSim. For this, two project cases, one with two parts, are made to investigate the approach for different wind speed regimes. In Project Case 1, the offshore site's actual wind data is used, including a wind regime with relatively high wind speeds and a mean wind speed of approximately 10.4 m/s. This project case includes a simulation with two different turbines with 5 MW and 15 MW installed capacity in Parts 1 and 2, respectively. The second project case, Project Case 2, is a virtual project case that includes wind data with lower wind speeds than the previous cases and a wind turbine of 15 MW. This wind regime includes a mean wind speed of approximately 7.7 m/s.

Three-dimensional micro-siting is an approach for the efficient design of wind farms. In this thesis, this approach includes variation of wind turbine hub heights. Simulation in the high wind speed regime originally indicated lower wake loss and higher AEP than simulation in the moderate wind speed regime. However, these increases are found to be marginal. On the other hand, the proposed 3D micro-siting could enhance the capacity density of prospective wind farms.

Analysis of the results from wind farms with 5 MW and 15 MW turbines indicate lower original wake losses with the 15 MW turbine. Regardless, the 3D micro-siting approach was more effective on the wind farms with the smaller turbine, indicating a more significant decrease in wake loss and an increase in capacity factor. The impact of the approach increased as the capacity density increased for all cases. In addition, this trend applies to both wake models, where the Larsen wake model indicated lower wake losses and higher AEP compared to the Jensen wake model. The parameters also change more significantly with the Larsen wake model.

The thesis's results indicate that the three-dimensional micro-siting approach is somewhat effective. This approach allows for the increase of capacity densities without significantly increasing the wake losses or decreasing the capacity factors. In fact, in some cases, these parameters can stay unaffected while increasing the capacity density with the 3D micro-siting approach included. Regardless, the approach in this study requires optimisation to limit the uncertainties in the results. In this way,

areas for offshore wind utilisation can be designed more efficiently.

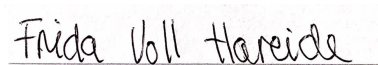


# Acknowledgements

This thesis is the final and concluding part of my master's degree in Renewable Energy at the University of Agder (UiA) in Grimstad. Before starting the master, I completed a bachelor's degree in Energy Technology at the Western Norway University of Applied Science in Bergen.

I would especially like to thank my supervisor, Professor Sathyajith Mathew (UiA), for the introduction to this topic, the guidance through the thesis process, the preliminary work, and the feedback while writing the thesis. I also want to thank Ghali Raja Yakoub for his help with preparing the input data and for his support in booting up the simulation in WindSim. This thesis could not have been completed without them.

Lastly, I want to thank my partner, family, and classmates for their significant support throughout the process. I look forward to the future and to starting my professional career.

A handwritten signature in black ink that reads 'Frida Voll Hareide'.

Frida Voll Hareide

University of Agder, Grimstad

26th of May, 2024



# Individual Declaration

The individual student is responsible for the use of legal tools, guidelines for their use and use of sources. The declaration is intended to make the students aware of their responsibility and the consequences of cheating. Missing statement does not release the students from their responsibility.

1.	I hereby declare that my thesis is my own work, and that I have not used other sources or received any help other than what mentioned in the thesis.	Yes
2.	<p><b>I further declare that this thesis:</b></p> <ul style="list-style-type: none"> <li>• Not have been used for another exam at another department/university/college in Norway or abroad.</li> <li>• Does not refer to other work without being stated.</li> <li>• Does not refer own previous work without being stated.</li> <li>• Include all references in the bibliography list.</li> <li>• Is not a copy, duplicate or copy of others work or answers.</li> </ul>	Yes
3.	I am aware that violation of the above is to be regarded as cheating and may result in annulment of examinations and exclusion from universities and colleges in Norway, see Universitets- og høyskoleloven §§4-7 og 4-8 og Forskrift om eksamen §§ 31.	Yes
4.	I am aware that all submitted assignments can be plagiarism checked.	Yes
5.	I am aware that the University of Agder will consider all cases where there is suspicion of cheating in accordance with the university college's guidelines for handling cases of cheating.	Yes
6.	I have been familiarised with the rules and guidelines for the use of sources and references on the library's website.	Yes



# Publishing Agreement

Authorisation for electronic publishing of the thesis. The author(s) hold the copyright to the thesis. This means, among other things, the exclusive right to make the work available to the public (Åndsverkloven. §2).

Assignments that are exempt from public disclosure or confidential/confidential will not be published.

I hereby give the University of Agder a free right to make the thesis available for electronic publication:	Yes
Is this thesis confidential?	No
Is the thesis exempt from public disclosure?	No



# Contents

Abstract . . . . .	iii
Acknowledgements . . . . .	iv
List of Figures . . . . .	xiv
List of Tables . . . . .	xvi
Nomenclature . . . . .	xvii
<b>1 Introduction</b>	<b>1</b>
1.1 Background . . . . .	1
1.2 Preliminary study . . . . .	4
1.3 Contribution to the Field . . . . .	4
<b>2 Literature review</b>	<b>6</b>
2.1 Wake Effect . . . . .	6
2.2 Wake models for wind farm planning . . . . .	8
2.2.1 The Jensen wake model . . . . .	8
2.2.2 The Larsen wake model . . . . .	8
2.2.3 The Frandsen wake model . . . . .	9
2.3 Comparison of wake models . . . . .	9
2.4 Micro-siting . . . . .	11
2.4.1 CFD based micro-siting . . . . .	12
2.5 Previous studies in variable hub heights . . . . .	12
2.5.1 Optimisation methods for micro-siting . . . . .	12
2.6 The use of WindSim . . . . .	13
2.7 Conclusion . . . . .	14
<b>3 Objectives of the Study</b>	<b>16</b>
3.1 Problem definition . . . . .	16
3.2 Research questions . . . . .	16
<b>4 Theory</b>	<b>18</b>
4.1 Wake Modelling . . . . .	18
4.1.1 Wake Model 1: The Jensen wake model . . . . .	18
4.1.2 Wake Model 2: The Larsen wake model . . . . .	19
4.1.3 Wake Model 3: The Ishihara wake model . . . . .	20

4.2	Actuator discs . . . . .	21
4.3	Rotor Thrust and Power . . . . .	21
4.4	Turbulence . . . . .	22
4.4.1	K- $\epsilon$ turbulence model . . . . .	22
4.5	Blockage Effect . . . . .	22
4.6	Annual Energy Production (AEP) . . . . .	23
4.7	Wind farm capacity factor . . . . .	23
4.8	Wind Speed Distribution . . . . .	23
4.8.1	Weibull Wind Distribution . . . . .	23
4.9	Computational Fluid Dynamics (CFD) analysis . . . . .	24
4.10	WindSim . . . . .	24
4.10.1	Terrain module . . . . .	25
4.10.2	Wind Fields module . . . . .	25
4.10.3	Objects module . . . . .	25
4.10.4	Results module . . . . .	26
4.10.5	Wind Resources module . . . . .	26
4.10.6	Energy module . . . . .	26
4.11	WindSim Express . . . . .	26
<b>5</b>	<b>Methodology</b>	<b>28</b>
5.1	Preparation of input data . . . . .	28
5.2	WindSim . . . . .	28
5.2.1	Preparatory modules . . . . .	29
5.2.2	Including actuator discs . . . . .	29
5.2.3	Wind Farm Design process . . . . .	30
5.3	Project Case 1-Southern Northsea II . . . . .	31
5.3.1	Wind resources at Southern Northsea II . . . . .	31
5.3.2	Part 1: Wind farms with 5 MW turbines . . . . .	33
5.3.3	Part 2: Wind farms with 15 MW turbines . . . . .	34
5.4	Project Case 2-Virtual wind farms . . . . .	36
5.4.1	Wind resources at Smøla wind site . . . . .	36
5.4.2	The Project Cases . . . . .	37
5.5	Computational parameters . . . . .	37
<b>6</b>	<b>Results and Discussions</b>	<b>40</b>
6.1	Southern Northsea II . . . . .	40
6.2	Onshore wind site at Smøla . . . . .	41
6.3	Three-dimensional micro-siting with 5 MW turbines . . . . .	43
6.3.1	Project Case 1: Part 1 . . . . .	43
6.4	Three-dimensional micro-siting with 15 MW turbines . . . . .	46
6.4.1	Project Case 1: Part 2 . . . . .	46
6.4.2	Project Case 2 . . . . .	50

6.5	Results evaluation . . . . .	53
6.6	Uncertainties . . . . .	54
<b>7</b>	<b>Conclusions</b>	<b>56</b>
7.1	Further Research . . . . .	57
	<b>References</b>	<b>59</b>
<b>A</b>	<b>Project Case 1 with 5 MW turbines</b>	<b>64</b>
A.1	Wake Model 1 results . . . . .	64
A.2	Wake Model 2 results . . . . .	65
<b>B</b>	<b>Project Case 1 with 15 MW turbines</b>	<b>66</b>
B.1	Wake Model 1 results . . . . .	66
B.2	Wake Model 2 results . . . . .	68
<b>C</b>	<b>Project Case 2 with 15 MW turbines</b>	<b>70</b>
C.1	Wake model 1 results . . . . .	70
C.2	Wake model 2 results . . . . .	71



# List of Figures

1.1	The historic development of onshore and offshore installations [GW] from 2001-2023. Image source: [3]. . . . .	2
1.2	The 20 identified areas for offshore wind utilisation. Image source: [5]. . . . .	3
1.3	Maps showing the degree of technical suitability and conflicts of interest for offshore wind utilisation around the Norwegian coastline. Image source: [6]. . . . .	3
2.1	The wake effect behind a wind turbine. Figure inspired by [9]. . . . .	7
2.2	The wake effect in an offshore wind farm. Image source: [11]. . . . .	7
2.3	The comparison of normalised wind speed for the Frandsen (grey line), Larsen (black line) and Jensen (red line) wake models and real measurements (black dots) at different downstream distances. Image source: [19]. . . . .	10
2.4	Comparison of power deficits for different wake models and SCADA from Gasiri wind farm at wind speeds from 6-9 m/s: (a) $U_0=6$ m/s, (b) $U_0=7$ m/s, (c) $U_0=8$ m/s and (d) $U_0=9$ m/s. Image source: [20]. . . . .	11
2.5	The normalised wind speed in the Bolund experiment, at a 5-meter height and wind direction of $239^\circ$ . Image source: [30]. . . . .	13
2.6	Normalised power production for Row 3 Lillgrund wind farm from a $120^\circ$ wind direction, including measured and modelled data. Image source: [31]. . . . .	14
2.7	Normalised power production for Row B in the Lillgrund wind farm from a $222^\circ$ wind direction, including measured and modelled data. Image source: [31]. . . . .	14
4.1	Schema for the Jensen Wake Model. Image source: [13]. . . . .	19
4.2	Schema for the Larsen Wake Model. Image source: [13]. . . . .	19
5.1	Placement of Southern Northsea II on the map. . . . .	32
5.2	The heat map for the wind speeds [m/s] at Southern Northsea II, at a height of 149 m. . . . .	32
5.3	The power density [ $W/m^2$ ] heat map for the relevant part of Southern Northsea II, at a height of 149 m. . . . .	32
5.4	The power and thrust coefficient curve for the 5 MW NREL reference turbine. . . . .	33
5.5	The $6 MW/km^2$ capacity density wind farm with 30 turbines of 5 MW. . . . .	34
5.6	The power and thrust coefficient curve for the 15 MW NREL reference turbine. . . . .	35
5.7	The $5.4 MW/km^2$ wind farm layout with 9 turbines of 15 MW. . . . .	36
5.8	The heat map for the wind speeds [m/s] in Project Case 2 at a height of 149 m. . . . .	37

5.9	The power density [ $W/m^2$ ] heat map for the site in Project Case 2 at a height of 149 m. . . .	37
6.1	The wind rose for the Southern Northsea II wind site, used in Project Case 1. . . . .	41
6.2	The Weibull distribution of wind (red line) fitted over the actual wind data (grey bars) at Southern Northsea II, used in Project Case 1. . . . .	41
6.3	The wind rose for the Smøla wind site used in Project Case 2. . . . .	42
6.4	The Weibull distribution of wind (red line) fitted over the actual wind data (grey bars) at Smøla wind site, used in Project Case 2. . . . .	42
6.5	The total AEP [MWh/y] at different capacity densities for the first part of Project Case 1. Both Wake Models 1 and 2 are included in the figure. . . . .	43
6.6	The capacity factor [%] at different capacity densities for the first part of Project Case 1. Both Wake Models 1 and 2 are included in the figure. . . . .	44
6.7	The wake loss [%] at different capacity densities for the first part of Project Case 1. Both Wake Models 1 and 2 are included in the figure. . . . .	45
6.8	The total AEP [MWh/y] at different capacity densities for the second part of Project Case 1. Both Wake Models 1 and 2 are included in the figure. . . . .	47
6.9	The capacity factor [%] at different capacity densities for the second part of Project Case 1. Both Wake Model 1 and 2 are included in the figure. . . . .	48
6.10	The wake loss [%] at different capacity densities for the second part of Project Case 1. Both Wake Models 1 and 2 are included in the figure. . . . .	49
6.11	The total AEP [MWh/y] at different capacity densities for Project Case 2. Both Wake Models 1 and 2 are included in the figure. . . . .	51
6.12	The capacity factor [%] at different capacity densities for Project Case 2. Both Wake Model 1 and 2 are included in the figure. . . . .	52
6.13	The wake loss [%] at different capacity densities for Project Case 2. Both Wake Models 1 and 2 are included in the figure. . . . .	53



# List of Tables

5.1	Data for Southern Northsea II [6]. . . . .	31
5.2	Pre-set properties for the 5 MW NREL Baseline Wind Turbine [62]. . . . .	33
5.3	Pre-set properties for the 15 MW NREL Baseline Wind Turbine [58]. . . . .	35
5.4	Description of the different project cases. . . . .	37
5.5	Input parameters in WindSim. . . . .	38
A.1	Results for Project Case 1 wind farms with 5 MW turbines with original hub height, including Wake Model 1 for wake simulation. . . . .	64
A.2	Results for Project Case 1 wind farms with 5 MW turbines with varying hub height, including Wake Model 1 for wake simulation. . . . .	64
A.3	Results for Project Case 1 wind farms with 5 MW turbines with original hub height, including Wake Model 2 for wake simulation. . . . .	65
A.4	Results for Project Case 1 wind farms with 5 MW turbines with varying hub height, including Wake Model 2 for wake simulation. . . . .	65
B.1	Results for Project Case 1 wind farms with 15 MW turbines with original hub height, including Wake Model 1 for wake simulation. . . . .	66
B.2	Results for Project Case 1 wind farms with 15 MW turbines with varying hub height, including Wake Model 1 for wake simulation. . . . .	67
B.3	Results from the wind farm layout with 12 $MW/km^2$ and 15 MW turbines. . . . .	67
B.4	Results from the wind farm layout with 15 $MW/km^2$ and 15 MW turbines. . . . .	67
B.5	Results for Project Case 1 with Wake Model 2, including the 15 MW turbine with original hub height. . . . .	68
B.6	Results for Project Case 1 with Wake Model 2, including the 15 MW turbine with varying hub height. . . . .	68
B.7	Results from the wind farm layout with 12 $MW/km^2$ and 15 MW turbines. . . . .	69
B.8	Results from the wind farm layout with 15 $MW/km^2$ and 15 MW turbines. . . . .	69
C.1	Results for the Project Case 2 wind farms with original hub heights and Jensen’s wake model included. . . . .	70
C.2	Results for the Project Case 2 wind farms with varying hub heights and Jensen’s wake model included. . . . .	70
C.3	The original hub height results for Project Case 2 with Wake Model 2. . . . .	71

C.4 The varying hub height results for Project Case 2 with Wake Model 2. . . . . 71



# Nomenclature

$C_P$	Power Coefficient
$C_T$	Thrust Coefficient
$2D$	Two-dimensional
$3D$	Three-dimensional
$AD$	Actuator disc
$AEP$	Annual Energy Production
$a$	Axial Induction Factor
$CD$	Capacity density
$CFD$	Computational Fluid Dynamics
$LCOE$	Levelized cost of energy
$NREL$	National Renewable Energy Laboratory
$RANS$	Reynolds Averaged Navier-Stokes
$SCADA$	Supervisory Control And Data Acquisition
$TI$	Turbulence Intensity
$WFDT$	Wind Farm Design Tool



# Chapter 1

## Introduction

### 1.1 Background

Today, most of the world's energy production comes from fossil energy resources. This energy production causes greenhouse gases to pollute the atmosphere, which feeds global warming. Renewable options for energy production are necessary to prevent this. Wind is a renewable, clean, and space-efficient energy resource which can contribute significantly to the green shift. The wind power technology is mature but has more potential for development [1]. Acceptable rated turbine capacities and efficiencies have been reached and continue to increase. For good reasons, global wind power capacity has increased significantly in the last decades. Wind power is consistent in the medium and long term, with low installation and operating costs compared to other energy sources. The lifetime of a wind farm is increasing, and it can today operate for 20-25 years with some adjustments and service [1].

Along with the increasing total wind power capacity is the increased capacity for offshore wind installations. Compared to an onshore wind farm, the main advantages of an offshore wind farm are generally higher wind speeds with more consistent direction [2]. These parameters generate higher wind farm capacity factors for offshore wind farms, indicating that fewer turbines are required to produce the same amount of energy as wind farms on land. Offshore wind turbines may also be more accessible to acceptance from the local population as they are more environmentally friendly and less visible. In addition, wildlife is less affected by offshore wind installations than the ones on land [2].

Figure 1.1 shows the historic developments of onshore and offshore wind installations globally from 2001-2023 as presented in the GWEC Global Wind Report 2024 [3]. The onshore installations are marked in green, and the offshore installations are marked in blue and are measured as installed capacity in GW. The figure shows that the total wind installations increase yearly, and the increase has been higher for the last couple of years. The total installations increased by 115 GW capacity from 2022 to 2023, resulting in 1021 GW in total installations. 11 GW of these 115 GW are offshore installations. This difference is significant compared to the numbers from 10 years ago, including a tenfold increase in offshore installations in these years.

Historic development of total installations (GW)

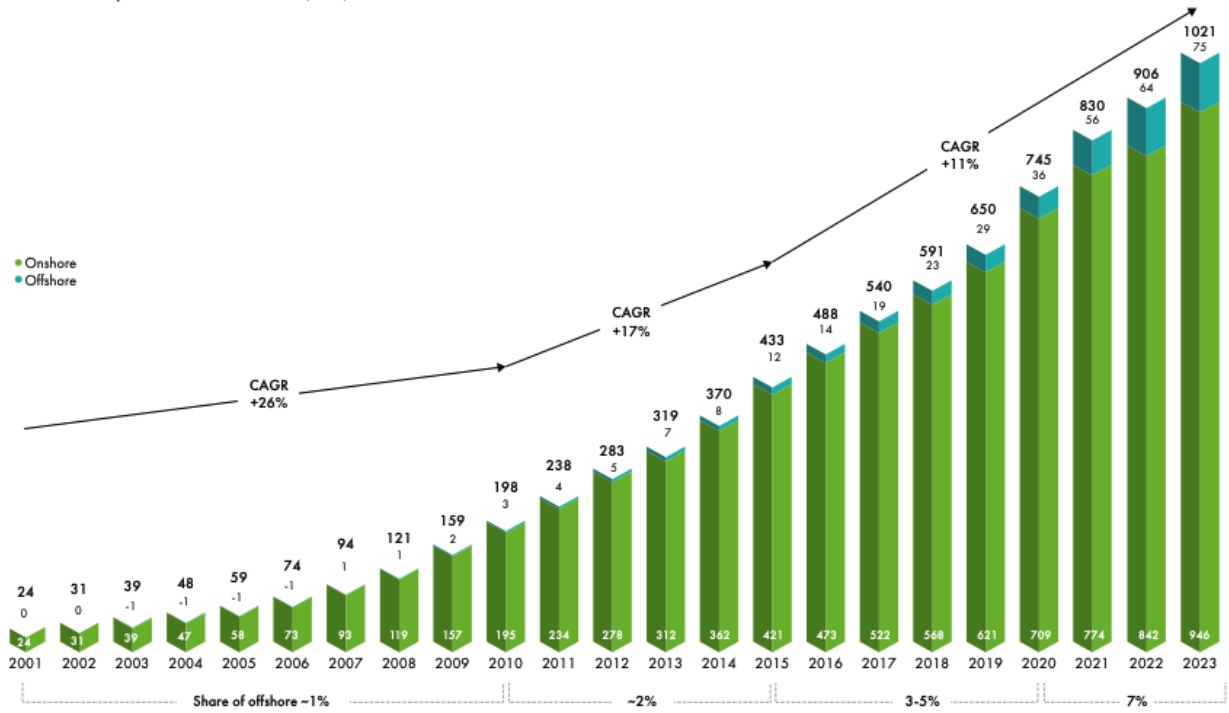


Figure 1.1: The historic development of onshore and offshore installations [GW] from 2001-2023. Image source: [3].

With a long coastline and coastal waters, Norway has large areas for industries at sea and offshore activities, such as offshore wind utilisation. The target from the Norwegian government is to install 30 GW of offshore wind capacity by 2040 [4]. To reach this target, the Norwegian Water Resources and Energy Directorate (NVE), commissioned by the government, has identified 20 new offshore areas usable for wind energy exploitation. Figure 1.2 shows these 20 offshore areas, placed around the entire Norwegian coastline, with the largest cluster in the southern part of the Norwegian coastal waters [5]. For each of these areas, impact assessments have been performed, in cooperation with other industries, on how the installation of wind turbines would affect the industries and the surrounding environment [4].

Figure 1.3 is a map from NVE [6] showing Norway and the offshore areas around the country. To the left is the technical suitability in the offshore areas, illustrated with dark colours for low and lighter colours for high suitability. The technical suitability is illustrated by the left side of the figure, including light colours close to the Norwegian coastline. The illustration indicates mid-high to high technical suitability for offshore wind utilisation in these areas. The illustration to the right in Figure 1.3 shows the degree of conflicts of interest in the same offshore areas. The light colours indicate low conflict, and the map shows generally low or middle-high conflicts of interest in the Norwegian offshore areas.



Figure 1.2: The 20 identified areas for offshore wind utilisation. Image source: [5].

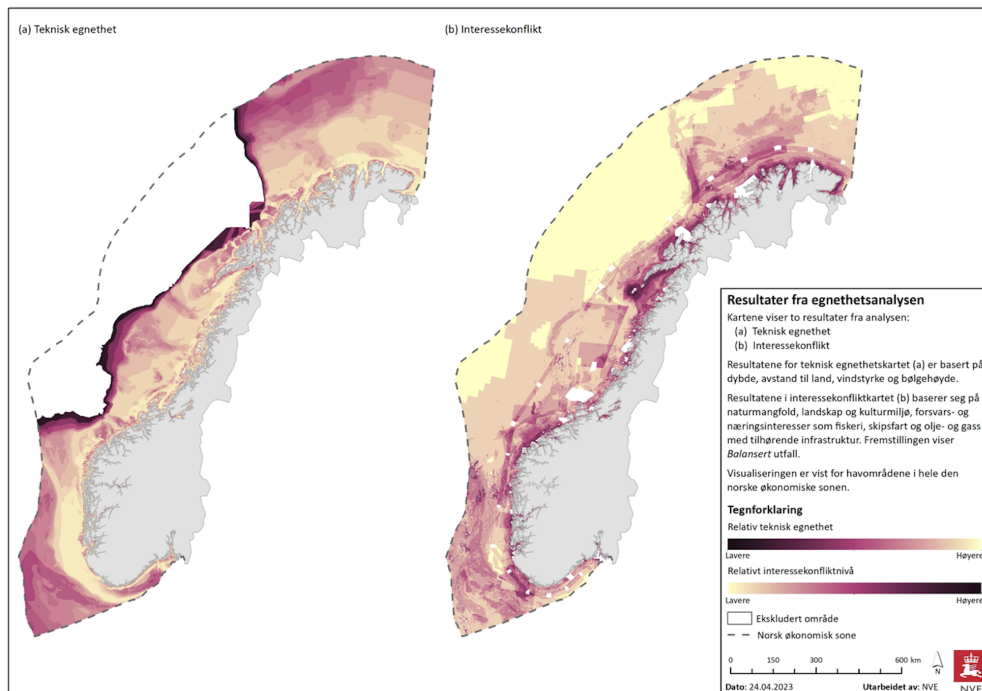


Figure 1.3: Maps showing the degree of technical suitability and conflicts of interest for offshore wind utilisation around the Norwegian coastline. Image source: [6].

The offshore wind farms are to be efficiently designed to exploit offshore wind areas and wind resources as best. Three-dimensional micro-siting is one approach for wind farm efficient design. Three-dimensional micro-siting involves changing the layout of a wind farm to maximise energy production and minimise the levelized cost of energy (LCOE). This process includes identifying the best coordinates at which the turbines



in a wind farm should be installed to gather the objective of maximised energy production and minimised LCOE. With increased energy production comes a decreasing wake effect, which causes losses in the wind farm. An efficient wind farm design includes determining the number of turbines in the wind farm, turbine type, turbine location, and the turbine hub height for each turbine. Because of space limitations, the turbines should be as close to each other as possible for the best power output in the limited area. For a three-dimensional micro-siting approach, the turbine type and hub height can vary within the same wind farm, which increases the wind farm complexity. The complexity will increase since dissimilar installations lead to different service needs and supply chain management [7].

This thesis deals with a three-dimensional micro-siting approach for efficient offshore wind farm design. The objective of this approach is to maximise the AEP and minimise the wake losses in offshore wind farms. This analysis is performed through wind farm simulations using WindSim software at the offshore wind site Southern Northsea II. NREL's 5 MW and 15 MW reference wind turbines, along with wind data from Southern Northsea II and Smøla, are used in the simulations. The simulations also include two wake models: the Jensen and Larsen wake models.

## 1.2 Preliminary study

The autumn semester of 2023 contained preparatory work for this master's thesis through a research project, resulting in a short report. This research project concerned a recursive micro-siting approach for wind farms for possible applications in offshore wind projects. The project included research on the micro-siting of wind farms and the CFD analysis method to get into the topic and learn how to use the WindSim software. The micro-siting was performed on an onshore site at Smøla in Norway, with varying elevations in the terrain. This approach could resemble a three-dimensional micro-siting approach with a turbine hub height variation. This preliminary study included a 5 MW turbine and wind data from Smøla, also included in this thesis.

## 1.3 Contribution to the Field

This master's thesis concerns the three-dimensional micro-siting of an offshore wind farm using the CFD-based software WindSim. Previous literature on micro-siting has mostly been analysed on onshore wind farms, but the literature on micro-siting of offshore wind farms is currently scarce. This thesis can enlighten the topic and investigate how micro-siting can benefit offshore wind farms, not only onshore farms, which is a more researched topic. Therefore, three-dimensional micro-siting on offshore wind farms, including turbine hub height variation, is to be further researched.



# Chapter 2

## Literature review

This chapter reviews previous studies on the micro-siting of wind farms and various aspects to consider in such wind farm design. Firstly, this chapter briefly describes the wake effect in wind farms. The following sections include a literature review of wake models for wind farm planning, a comparison of wake models, and a review of the micro-siting topic. Lastly, different methods for optimising these micro-siting approaches and previous studies in turbine hub height variation are reviewed.

### 2.1 Wake Effect

Wind energy exploitation includes extracting energy from the wind using a wind turbine [8]. This energy extraction reduces the wind speed and swirls the airflow behind the rotor. This reduction in wind speed is called the wake effect of a wind turbine, which affects the surrounding wind turbines in a wind farm and gives so-called wake losses. Wakes are characterised as near and far wakes. The far wake is the most important in a wind farm as wake losses reduce the energy production potential, meaning the turbines produce less energy than they would have initially [8]. The wake effect for one wind turbine is described in Figure 2.1. Equation 2.1 formulates the normalised wind speed deficit [9]. The figure shows that the wake expands as the distance behind the wind turbine rotor increases.  $U$  represents the free stream wind speed and  $V$  represents the wind speed at a distance  $x$  behind the turbine rotor [10]. In calculations of losses due to the wake effect, reduced wakes is calculated off hub height as the wake is modelled rotational symmetric with the  $x$ -axis.

$$\delta V = \frac{(U - V)}{U} \tag{2.1}$$

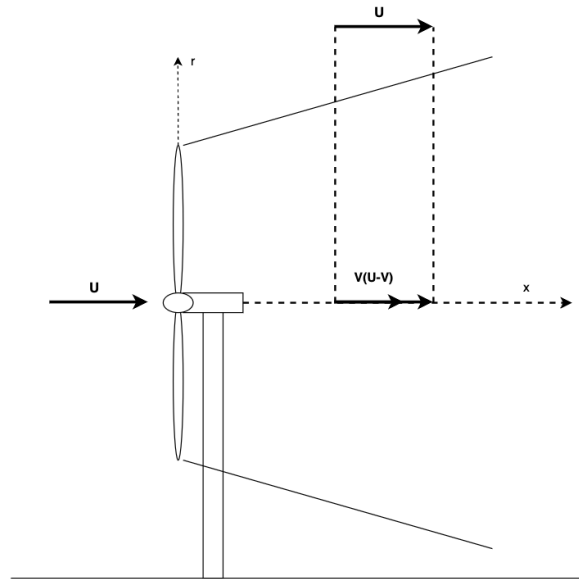


Figure 2.1: The wake effect behind a wind turbine. Figure inspired by [9].

Figure 2.2 shows the wake effect in an offshore wind farm [11]. Turbine A disrupts the airflow, which causes reduced wind speed behind the turbine in the region where Turbine B is placed. The lower wind speed for Turbine B due to wake leads to a lower power output. Offshore areas include limited surface roughness, meaning less elevation in the sea bottom for bottom fixed turbines and the water surface for the floating turbines. Due to limited surface roughness in offshore areas, less turbulence is produced in offshore wind farms compared to wind farms on land. With lower turbulence, there is a slower recovery of wakes, in addition to making the wakes longer. Because of this, the wake effect can be especially enhanced for offshore wind farms and requires more efficient design of the wind farms and optimisation [11].

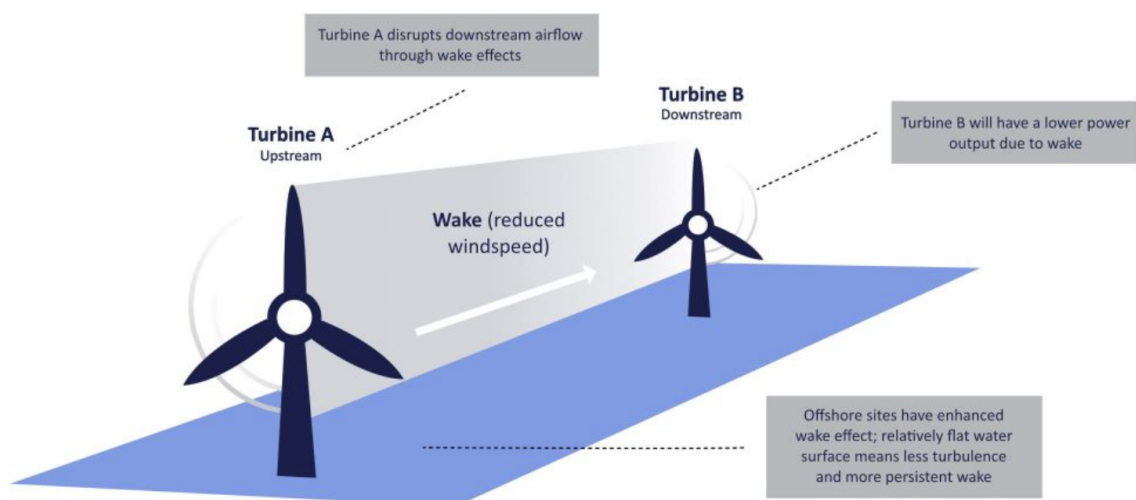


Figure 2.2: The wake effect in an offshore wind farm. Image source: [11].

## 2.2 Wake models for wind farm planning

Wake modelling is significant in wind resource assessment and wind farm planning. A wake model simulates the wake losses by each turbine in near and far wake and is significant in wind farm planning to decrease the power loss [8]. The suitability of the wake models varies depending on the wind conditions at the wind site. The following sections review some common wake models and studies that compare these models against actual wind farm measurements of wake loss.

### 2.2.1 The Jensen wake model

The Jensen wake model is a simple and relatively accurate wake model commonly used for wake simulations [8]. The Law of Momentum Conservation implies a linearly expanding wake behind the turbine, and the wake speed deficit depends on the axial distance and wake decay [8] [12]. The diameter of the wake ( $D_w$ ) as it expands behind the turbine rotor dependent on the downstream turbine distance ( $x$ ) is formulated in Equation 2.2 [12]. In this equation,  $D$  is the turbine diameter, and  $k_w$  is the wake decay. In [13]  $k_w=0.04$  for offshore wind farms.

$$D_w(x) = D \left( 1 + 2k_w \frac{x}{D} \right) \quad (2.2)$$

Section 4.1.1 in Chapter 4 elaborates on the Jensen wake model and how it is implemented in the simulations in WindSim for this study.

### The Jensen wake model with a Gaussian improvement

The Jensen wake model is commonly used for its simplicity and accuracy and since it captures the overall behaviour of airflow behind a turbine rotor well but neglects the details [14]. However, the wake model is less effective at low wind speeds and near wakes and fails to capture the radial dependence of wake. Therefore, the energy production predictions in a wind farm are sensitive to wind direction [14]. Researchers work on developing the wake model to be better in all aspects. The Jensen-Gaussian wake model is a version of the Jensen wake model where the top-hat distribution in a Gaussian wake model replaces the Jensen top-hat distribution [15]. This change results in a Jensen wake model with a Gaussian-shaped speed deficit, which is two-dimensional [14]. The wake radius calculation is similar to the Jensen wake model, but the coefficient  $k$  is corrected for turbulence intensity [16].

### 2.2.2 The Larsen wake model

With the Larsen wake model, wakes are simulated as a linear perturbation on the mean wind field but include individual modelling of the wake flow field termed by non-linear simulations [17]. The simulation of the wakes includes an approximation of the shear layer and symmetric wake flow field. Also, a function of axial and radial distance,  $x$  and  $r$ , respectively, indicate the model's wind speed deficit [12] [17]. This indicates a more complex wake model than the Jensen wake model, as the wake deficit is only dependent on the axial distance [17]. Equation 2.3 presents the wake expansion behind the rotor with the Larsen wake model [12].

$$D_w(x) = 2 \left( \frac{35}{2\pi} \right)^{\frac{1}{5}} (3c_1^2)^{\frac{1}{5}} [C_T(U_{in})Ax]^{\frac{1}{3}} \quad (2.3)$$

In this equation,  $c_1$  represents a mixing length,  $C_T$  is the thrust coefficient,  $U_{in}$  is the inflow wind speed, and  $A$  is the cross-section area. Section 4.1.2 in Chapter 4 elaborates on the Larsen wake model and its implementation in the WindSim simulation software.

### 2.2.3 The Frandsen wake model

The Frandsen wake model is based on momentum analysis, including the Momentum Conservation Law of flow over a control volume for one or several wind turbines [18]. In this analysis, the wake speed is directly related to the thrust coefficient and a given thrust coefficient is calibrated by the expansion of the wake area. The control volume is cylindrical with a constant cross-sectional area, equal to the wake area and horizontal axis parallel to the mean wind vector [13]. The wake expansion behind the rotor with the Frandsen wake model is formulated in Equation 2.4 [12]. In this equation, the wake expansion is formulated as a function of the downstream turbine distance, where  $\alpha=0.7$ ,  $D$  is the turbine diameter, and  $k=3$  in [12]. In this equation,  $\beta$  is the wake expansion parameter formulated in Equation 2.5, where  $C_T$  is the thrust coefficient and  $U_{in}$  is the inflow wind speed.

$$D_w(x) = D \left( \beta^{\frac{k}{2}} + \alpha \frac{x}{D} \right)^{\frac{1}{k}} \quad (2.4)$$

$$\beta = \frac{1 + \sqrt{1 - C_T(U_{in})}}{2\sqrt{1 - C_T(U_{in})}} \quad (2.5)$$

## 2.3 Comparison of wake models

In [19], the three wake models, Frandsen, Larsen and Jensen wake model, are compared to actual lidar measurements from an onshore wind farm in China and evaluated at different distances from the turbine rotor. Figure 2.3 presents this study graphically with the normalised wind speed at different downstream distances ranging from 2D-6D. As shown in the figure, the velocity lateral distribution in the wake for the Jensen and Frandsen wake models is assumed uniform, which is not the case in actual measurements. Therefore, in this case, a modification of the Jensen wake model is needed to match the measurements. For the Larsen model, the velocity deficit in the wake centre is underestimated but describes the radial variation of velocity. The prediction of the wake models has higher precision in far wake. The Larsen and Frandsen wake models predict generally wider wake widths than the actual measurements. The three wake models underestimate the velocity deficit but are more accurate for the far wakes [19].

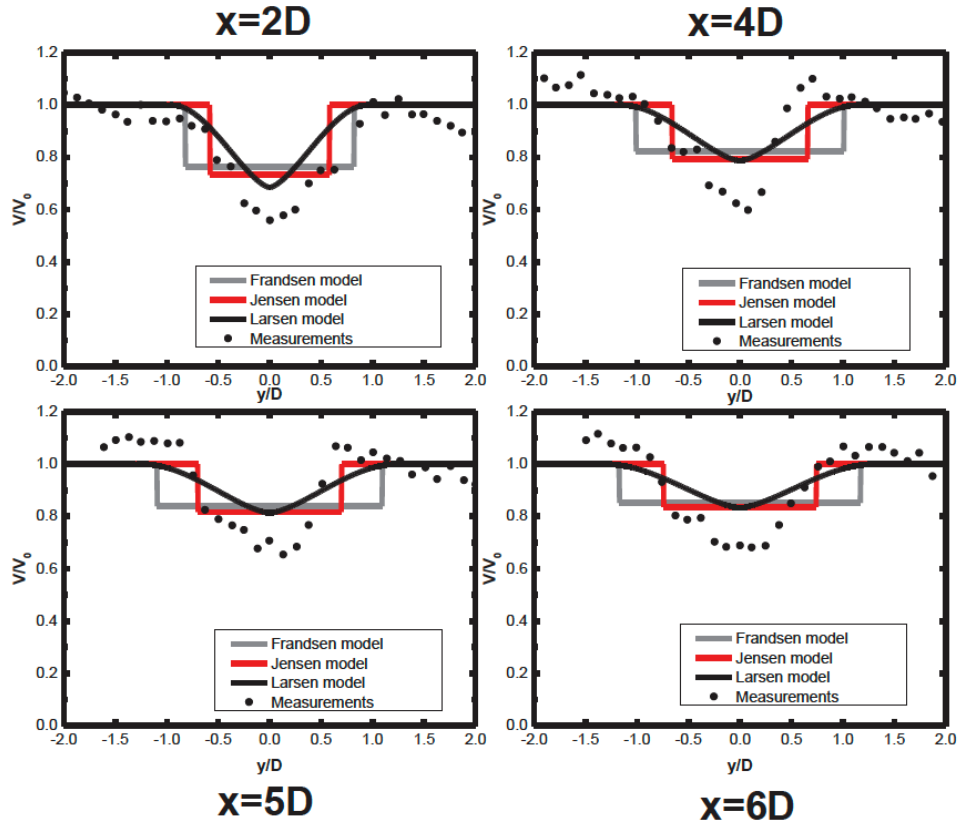


Figure 2.3: The comparison of normalised wind speed for the Frandsen (grey line), Larsen (black line) and Jensen (red line) wake models and real measurements (black dots) at different downstream distances. Image source: [19].

Four wake models are compared to SCADA measurements from turbine pairs in the Gasiri wind farm in [20]. Figure 2.4 presents the relative wind direction versus relative power comparison for the Jensen, Frandsen, Larsen and Jensen-Gaussian wake models for wind speeds from 6-9 m/s. The distance between the turbines is  $3.8D$ , wind direction  $\theta_a=30^\circ$  and turbulence intensity equal 0.14. Figure 2.4 shows that the Jensen wake model generally underestimates the wind speed, but the power deficit is calculated as larger than the wind speed deficit. Because of this, the Jensen wake model can give satisfactory results in simulation. In this study, the Larsen wake model generally calculates a lower power deficit than the other three wake models. The Jensen and Jensen-Gaussian wake models agree the best with the SCADA data in Figure 2.4, and they get more accurate as the wind speed increases [20].

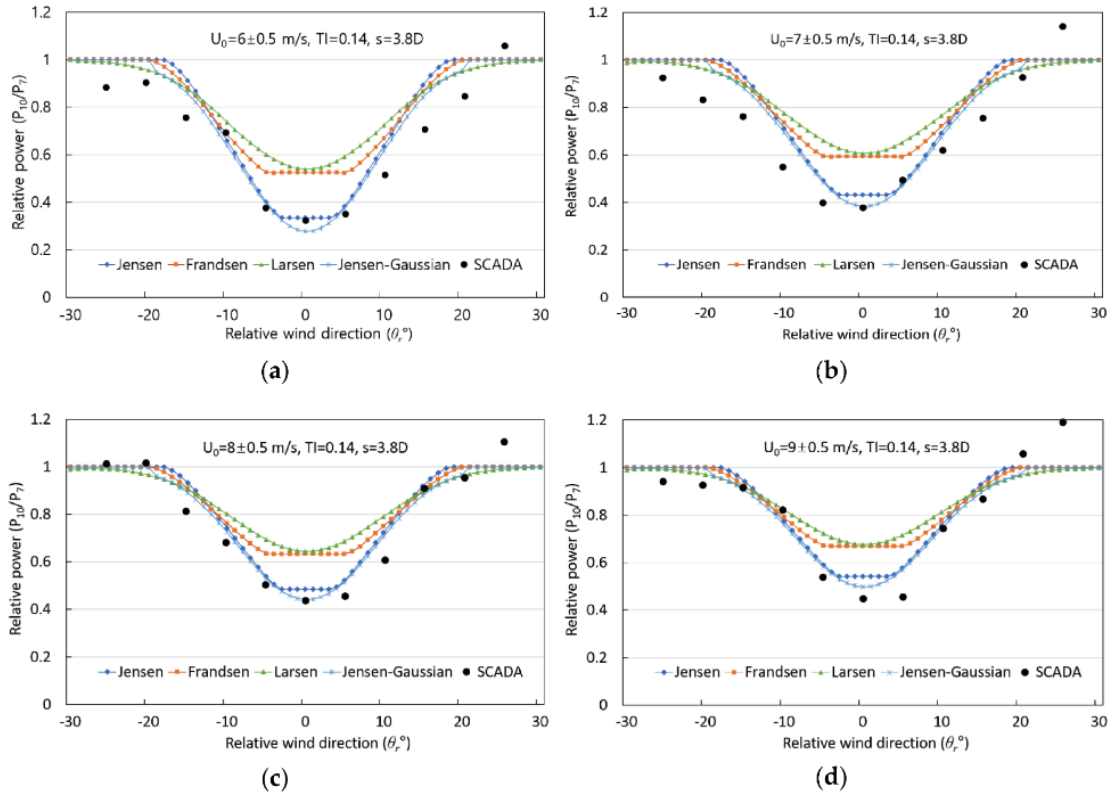


Figure 2.4: Comparison of power deficits for different wake models and SCADA from Gasiri wind farm at wind speeds from 6-9 m/s: (a)  $U_0=6$  m/s, (b)  $U_0=7$  m/s, (c)  $U_0=8$  m/s and (d)  $U_0=9$  m/s. Image source: [20].

## 2.4 Micro-siting

Micro-siting has been a common method for efficiently designing wind farms for the last couple of years [21]. Micro-siting can happen in a two-dimensional and three-dimensional approach. Two-dimensional (2D) micro-siting deals with wind farm optimisation by changing the turbine position in X and Y directions. For the three-dimensional approach (3D), the optimisation also concerns the change in the position of the Z-direction, meaning changing the turbine hub height. This approach will extract more power than the 2D approach with less capital cost. The main goal of this method is to minimise the total wake loss of a wind farm, maximise the annual energy production, and decrease the costs [21]. Today, 2D micro-siting is the more common method, meaning that 3D micro-siting requires more testing for the future.

In addition to changing the turbine hub height and position, it can be advantageous to a non-uniform wind farm, including varying the turbine type, meaning size and power output, and the number of turbines in the wind farm [22][23]. With bigger turbines, fewer turbines are needed at a site to gather the same installed capacity as smaller ones [22]. Using bigger turbines would, therefore, be advantageous since fewer turbines result in higher capacity factors and less wake effect. On the other hand, a non-uniform wind farm can increase the complexity of a wind farm since different types of turbines have different service needs, and the supply chain management is different. The choices for a non-uniform wind farm also depend on the costs, as bigger turbines cost more than smaller ones [22].



### 2.4.1 CFD based micro-siting

Some studies have been on CFD-based micro-siting before, but for onshore sites and often with a complex terrain [24] [25]. These studies use the RANS equations with the  $k-\epsilon$  turbulence model as the turbulence closure. These studies implement versions of the Jensen wake model for the wake loss simulations, such as the Jensen-Gaussian [24] and the Jensen-Katic wake model [25]. For example, CFD simulations have been evaluated in [24] to actual measurements in a wind tunnel and gave good results with a small number of errors with an average of 2.6 % [24]. This result means that the CFD-simulated wind speeds correspond to the measured wind speeds in the wind tunnel. Therefore, CFD is evaluated as accurate in simulating the vertical distribution of the mean wind speed along with the surface, which is a natural complex [24]. WindSim is a CFD-based software, which is elaborated on in sections 4.9 and 4.10.

## 2.5 Previous studies in variable hub heights

In [26], three-dimensional micro-siting is performed by using CFD analysis in WindSim. In this thesis, both two-dimensional and three-dimensional micro-siting were researched in complex terrain. The 2D micro-siting included turbine placing, one by one, at the points with the highest power densities. This 2D micro-siting resulted in a capacity factor of 31 % and a minimum wake loss of 5.6 %. For the 3D micro-siting, the hub heights varied between 119-166 m. The highest turbines gathered the biggest energy production, and the turbines with lower hub heights had a marginal decrease in efficiency compared to the other turbines. The lower turbines, on the other hand, cost less than bigger turbines. The conclusion included, by analysing the simulation results, that 3D micro-siting may not be necessary for energy production output in complex terrains with lots of variation in elevation. However, lower towers indicate reduced costs [26].

### 2.5.1 Optimisation methods for micro-siting

The optimisation of wind farm layout and turbine hub height with a novel wake model using a genetic algorithm has yielded good results. In [27], the created model increased the power output by 154 % by optimising the turbine hub height and wind farm layout simultaneously. For comparison, an optimisation of the two factors independently could increase the power output by 55 % and 79 %, respectively [27]. A simultaneous wind farm and turbine hub height optimisation could, therefore, severely impact the wind farm power output, such as in study [27]. In this case, the wake model was improved by 3D artificial neural network (3D-ANN) technology for more accuracy and reduced computational time and costs [27].

Micro-siting can be performed using a two-level approach to optimise a wind farm even more. In [28], a two-level approach is used to find the optimal wind farm solution easier. In this study, a wind farm is separated into blocks of the same size, with a multi-objective algorithm to optimise each block. A multi-objective algorithm can solve problems with multiple objective functions and optimise these simultaneously [29]. This

algorithm creates different block candidates for each block, which is used as a compound-level algorithm to optimise the entire wind farm [28]. The study included 24 cases with different wind conditions, number of turbines, choices and objective combinations. The approach gave good results and is an improvement compared to the usual one-level approach.

## 2.6 The use of WindSim

A team from WindSim AS have validated the WindSim software by validating the mean wind speed and turbulence model used for actual measurements at Bolund Hill [30]. Risø provides the input data and measurements. This project showed that WindSim generally underestimates turbulence. Other than that, the errors were among the lowest gathered for this type of test for Bolund Hill [30]. Figure 2.5 shows the results of different models in the Bolund experiment submitted to the Bolund Blind Comparison. The figure shows the normalised wind speed from a wind direction of  $239^\circ$  at a 5-meter height. The black boxes are the actual measurements, the pink line is the results from WindSim, and the remaining lines are from other models in this experiment. The figure shows that the WindSim results correspond to the actual measurements [30].

In [31], the WindSim software performs CFD analysis to compare analytical wake and actuator disc models. The compared models are an old actuator disc implementation with uniform force distribution, a new actuator disc model where the forces and power are calculated directly for each disc cell, and the other two models, the Jensen and Larsen wake models. Figures 2.6 and 2.7 show the results from this comparison on normalised power production for two rows in the wind farm, meaning Rows 3 and B [31]. In both figures, 3/4 of models generally underestimate the power production. The New ACD model corresponds to some measurements and overestimates the rest. In the cases in Figures 2.6 and 2.7, the Larsen wake model underestimates less than the other models, with the best correspondence in Figure 2.6.

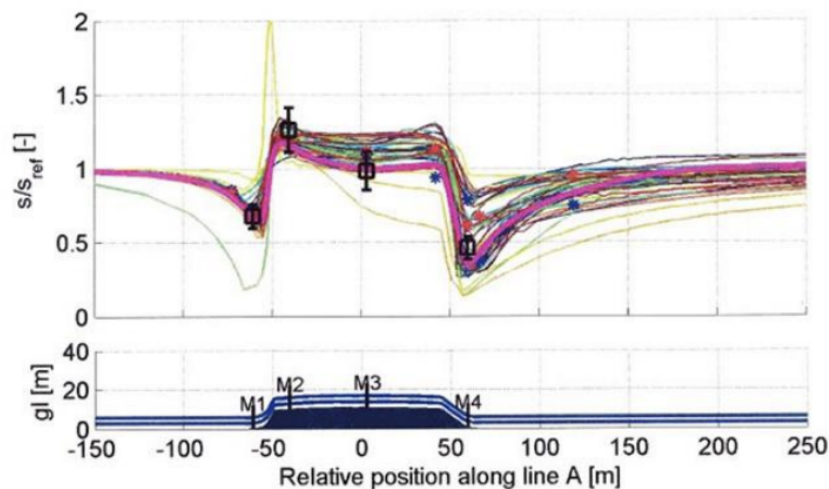


Figure 2.5: The normalised wind speed in the Bolund experiment, at a 5-meter height and wind direction of  $239^\circ$ . Image source: [30].

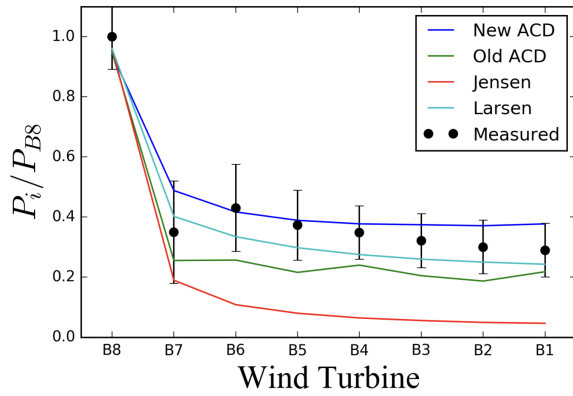


Figure 2.6: Normalised power production for Row 3 Lillgrund wind farm from a  $120^\circ$  wind direction, including measured and modelled data. Image source: [31].

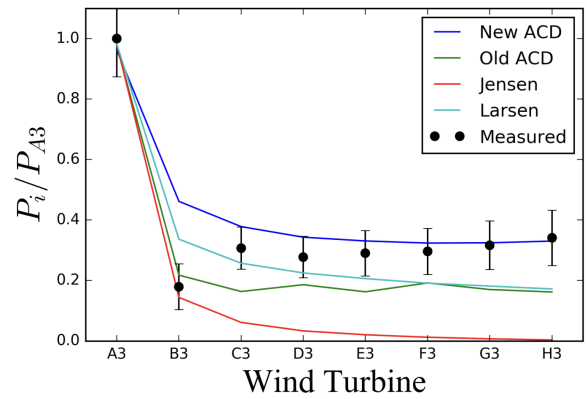


Figure 2.7: Normalised power production for Row B in the Lillgrund wind farm from a  $222^\circ$  wind direction, including measured and modelled data. Image source: [31].

## 2.7 Conclusion

Through this literature review, several common wake models have been presented and compared to each other, in addition to actual measurements at different sites. However, the Jensen wake model, or a version of the model, is commonly used in studies that include micro-siting and CFD analysis. The reviewed literature indicates that the fit of the different wake models varies depending on the wind conditions at the specific site and method used, and the Larsen wake model also gathered acceptable results in some of the studies. Through several reviewed studies on onshore wind farms, CFD implementation, including WindSim simulations, has been validated as suitable for onshore wind resource assessment with values corresponding to actual measurements. This includes the actuator discs function in WindSim. The 3D micro-siting with the variable hub height concept has yielded good results in the simulation of onshore wind farms. In most cases, this includes optimisation of the wind farm layout using different algorithms, which is shown to be better than the implementation of the variable hub height concept alone. There is a lack of studies on implementing 3D micro-siting on offshore wind farms in the current literature, which needs further research.



## Chapter 3

# Objectives of the Study

### 3.1 Problem definition

This study's objective is to maximise offshore wind farm's annual energy production (AEP) using a three-dimensional micro-siting approach. This approach includes placing turbines at a wind site in the areas with the highest power density, one by one, according to the wake effects. Further, the wind farm layout will be changed by varying the turbine hub heights to reduce the effect of the wake. The approach includes the turbine hub height variation in wind farms with different capacity densities and characteristics.

The three-dimensional micro-siting in this study uses the offshore area Southern Northsea II as the basis for the simulations, including its technical and wind data and the 5 MW and 15 MW NREL reference turbines. A virtual case with lower wind speeds is also performed to investigate the method further, using onshore wind data from a site at Smøla in northwestern Norway with the geographical data from Southern Northsea II. For all cases, the wind resources are analysed using two different wake models: the Jensen and Larsen wake models. The research questions formulated for the study are given below.

### 3.2 Research questions

This master's thesis will focus on the following research questions:

- RQ1:** How can the wake loss be minimised and annual energy production (AEP) be maximised by applying the three-dimensional micro-siting in high and moderate wind speed regimes?
- RQ2:** How do the wind farm's capacity density and the turbine's rated capacity affect the AEP and wake losses in a three-dimensional micro-siting approach?
- RQ3:** How would the above analysis on three-dimensional micro-siting be affected by the model chosen for the wake estimation?



# Chapter 4

## Theory

This chapter describes the theoretical considerations significant to this thesis. The coming sections include theory on wake modelling, actuator discs, wind speed distribution, CFD analysis, the WindSim software, and significant characteristics in wind resource assessment. This includes equations used to calculate the implemented parameters in the WindSim simulations.

### 4.1 Wake Modelling

Mathematical wake models have been developed for wind farm studies and simulation to predict the wake size and energy losses due to the wake effect. In this way, predictions of the energy production of a wind turbine can be made. The sections below describe the available options for wake simulation in WindSim: the Jensen, Larsen, and Frandsen wake models. These are called Wake Models 1, 2 and 3, respectively, in WindSim. A wind farm includes several wind turbines, which indicate different wakes for each turbine and multiple wakes affecting each other. The multiple wake model is based on the sum of squares in the simulations.

#### 4.1.1 Wake Model 1: The Jensen wake model

The Jensen wake model is commonly used in studies for both onshore and offshore wind farms [28] [32]. The reason for this is that the model gives low computational costs and is simple in computation [22]. The model accuracy is also relatively high, especially in the far wake region [8] [33]. The Jensen wake model assumes a linearly expanding wake with a velocity deficit dependent on the distance behind the rotor. The model also assumes a turbulent wake and neglects tip vortex contribution. The Jensen wake model is derived by downstream wind momentum conservation since the model handles wake as turbulent [33]. Figure 4.1 shows the linearly expanding wake with the Jensen wake model. Equation 4.1 presents the velocity in the wake with the Jensen wake model. In the figure and equation,  $C_T$  is the trust coefficient,  $z$  is the turbine hub height,  $z_0$  is the roughness height,  $D_0$  is the rotor diameter,  $D_w$  is rotor diameter at distance  $x$ ,  $A=0.5$ , and  $u$  is the velocity of the free stream. The wake decay in the Jensen wake model is represented by  $\alpha$  and can be calculated by Equation 4.2 [13]. The wake decay typically range from 0.04 to 0.075 [9].

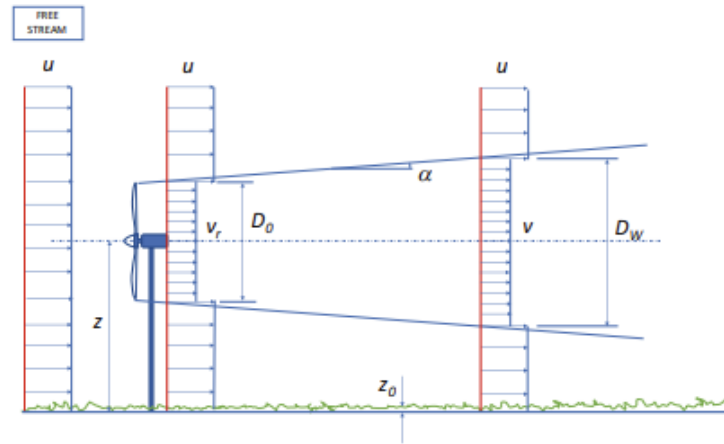


Figure 4.1: Schema for the Jensen Wake Model. Image source: [13].

$$\delta v = \frac{(1 - \sqrt{(1 - C_T)})}{(1 + (\frac{2\alpha x}{D_0}))^2} \quad (4.1)$$

$$\alpha = A / \ln(\frac{z}{z_0}) \quad (4.2)$$

#### 4.1.2 Wake Model 2: The Larsen wake model

The Larsen wake model considers a wind turbine wake a disturbance of a mean wind flow [17]. This disturbance of the mean wind flow may include wake shear from upstream emitted wakes and conventional shear. Due to the conventional shear and wake shear, downstream in the wind farm is developed, which decreases as the distance from the wind turbines increases but simultaneously expands in space [17]. Figure 4.2 shows the expansion of the wake with the Larsen wake model. In the figure,  $z$  is the turbine hub height,  $z_0$  is the roughness height, and  $x$  and  $r$  are axial and radial coordinates, respectively [13].

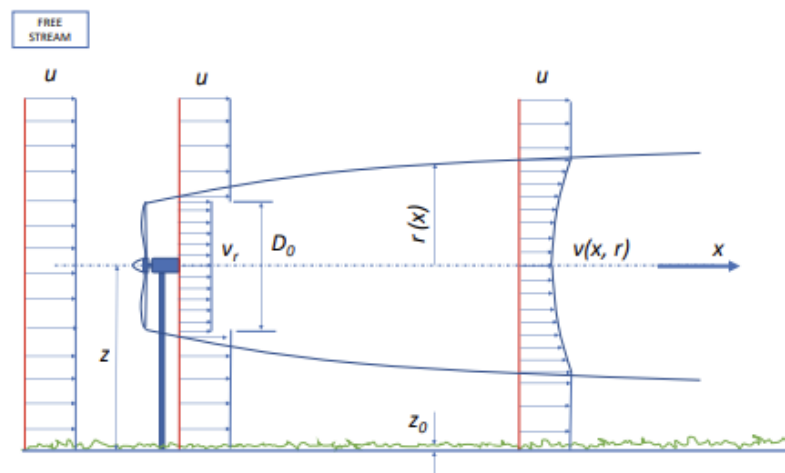


Figure 4.2: Schema for the Larsen Wake Model. Image source: [13].



Equation 4.3 presents the velocity in the wake in the Larsen wake model [9]. The equation includes the parameters calculated by Equations 4.4, 4.5, 4.6, 4.7, and 4.8 [9].

$$\delta V = \frac{1}{9}(C_T A_r x^{-2})^{\frac{1}{3}} [r^{\frac{3}{2}} (3C_1^2 C_T A_r x)^{-\frac{1}{2}} - (\frac{35}{2\pi})^{\frac{3}{10}} (3C_1^2)^{-\frac{1}{5}}]^2 \quad (4.3)$$

$$A_r = \pi \frac{D_0^2}{4} \quad (4.4)$$

$$C_1 = (\frac{D_0}{2})^{\frac{5}{2}} (C_T A_r x_0)^{-\frac{5}{6}} \quad (4.5)$$

$$x_0 = 9.5 \frac{D_0^4}{(2R_{95})^3} - 1 \quad (4.6)$$

$$R_{95} = 0.5(R_{nb} + \min(z, R_{nb})) \quad (4.7)$$

$$R_{nb} = \max(1.08D_0, 1.08D_0 + 21.7D_0(I_a - 0.05)) \quad (4.8)$$

In these equations,  $C_T$  is the thrust coefficient,  $A_r$  is the rotor swept area,  $D_0$  is the rotor diameter,  $I_a$  is the ambient turbulent intensity at hub height,  $R_{nb}$  is a corrected wake radius, and  $z$  is the turbine hub height.

### 4.1.3 Wake Model 3: The Ishihara wake model

The Ishihara wake model is based on the momentum of axial symmetry flow and the turbine drag force-loss of momentum flux relation [34]. In addition, the model considers the turbulence effect on the wake recovery, which depends on the turbulence generated by the turbine [34] [35]. The Ishihara wake model depends on the downstream distance from the wind turbine, the Atmospheric and rotor-generated turbulence, and is not constant [35]. Equations 4.9, 4.10, 4.11, and 4.12 present the velocity in the wake in Ishihara wake model [9].

$$\delta V = \frac{C_T^{\frac{1}{2}}}{32} (\frac{1.666}{k_1})^2 (\frac{x}{D})^{-p} \exp(\frac{-r^2}{b^2}) \quad (4.9)$$

$$b = k_1 \frac{C_T^{\frac{1}{4}}}{0.833} D^{(\frac{1-p}{2})} x^{\frac{p}{2}} \quad (4.10)$$

$$p = k_2(I_a + I_w) \quad (4.11)$$

$$I_w = k_3 (\frac{C_T}{\max(I_a, 0.03)}) (1 - \exp(-4(\frac{x}{10D})^2)) \quad (4.12)$$

In these equations,  $C_T$  is the thrust coefficient,  $D$  is the rotor diameter,  $I_a$  is the ambient turbulent intensity at hub height,  $I_w$  is the mechanical turbulence generated,  $k_1=0.27$ ,  $k_2=6$ , and  $k_3=0.004$  [9].  $p$  is regarded as a function of turbulence and shows the rate of wake recovery [34].

## 4.2 Actuator discs

An actuator disc is often used to simplify wind farm modelling, especially in CFD simulations. An actuator disc is a penetrable disc for the air to pass through, representing a wind turbine's swept rotor area (A) [36]. The forces directed against the axial wind direction are used by the cells that cover area A [37]. The thrust force  $F_i$  in the actuator disc model is calculated from Equation 4.13.

$$F_i = \frac{1}{2} \rho A_i \left( \frac{U_{1,i}}{1 - a_i} \right)^2 C_T(U_{1,i}) \quad (4.13)$$

In this equation,  $U_{1,i}$  represents the wind speed at the  $i$ -th cell of the disc perpendicular to the disc,  $A_i$  is the specific surface area,  $a_i$  is the axial induction factor,  $C_T(U_{1,i})$  is a modified version of the thrust coefficient dependent on the disc velocity  $U_{1,i}$ , and  $\rho$  is the air density. The thrust coefficient  $C_T$  and  $U_1$  is presented in Equations 4.14 and 4.15, which lead to Equation 4.16 [37].

$$C_T = 4a(1 - a) \quad (4.14)$$

$$U_1 = (1 - a)U_\infty \quad (4.15)$$

$$U_1 = \frac{1}{2} U_\infty (1 + \sqrt{1 - C_T(U_\infty)}) \quad (4.16)$$

This thesis implements actuator discs to refine non-AD simulations to implement losses and give more realistic simulations.

## 4.3 Rotor Thrust and Power

Equation 4.17 presents the relationship between the power coefficient and axial induction factor [38]. The power coefficient ( $C_P$ ) is the ratio between the extracted wind turbine power and the available energy in the wind stream [39]. Equation 4.18 presents the relationship between the thrust ( $C_T$ ) coefficients and the axial induction factor (a) [40]. The thrust coefficient describes the relationship between the thrust and dynamic forces.

$$C_P = 4a(1 - a)^2 \quad (4.17)$$

$$C_T = 4a(1 - a) \quad (4.18)$$

Factor  $a$  in the equations represents the axial induction factor and indicates how much the turbine slows the upstream wind velocity [38]. Both coefficients are a number between 0-1 [41]. The maximal theoretical  $C_P$  is 16/27 or 59.26 %, which is also called Betz' limit [42]. At maximum power output, which includes the axial induction factor (a) equal to  $\frac{1}{3}$  [41]. The thrust coefficient  $C_T$  is equal to 8/9 in this case [41].

## 4.4 Turbulence

The occurrence of turbulence in the wind is defined as fluctuations in wind speed caused by the dissipation of wind energy from kinetic to thermal energy [43]. This dissipation includes the creation and destruction of small wind gusts. Turbulence can seem random but happens distinctly. Therefore, the turbulence occurrence and behaviour can be modelled with different wind characterisation properties like fluid density, turbulence intensity (TI), turbulent kinematic viscosity, kinetic energy, and dissipation rate [43]. Turbulence in an airflow reduces the available power and creates fatigue loads on a wind turbine [44]. Equation 4.19 presents the turbulence intensity, which includes the standard deviation ( $\sigma_u$ ), presented by Equation 4.20 [43].

$$TI = \frac{\sigma_u}{U} \quad (4.19)$$

$$\sigma_u = \sqrt{\frac{1}{N_s - 1} \sum_{i=1}^{N_s} (u_i - U)^2} \quad (4.20)$$

### 4.4.1 K- $\epsilon$ turbulence model

The k- $\epsilon$  turbulence model is a commonly used Eddy viscosity model to simulate mean flow characteristics in turbulence flow conditions [45]. An Eddy viscosity model, such as this one, is also used for Reynolds stresses calculation. The k- $\epsilon$  turbulence model is described in Equations 4.21, and 4.22 [37].

$$(\rho k), t + (\rho U i k - \frac{\rho v_t}{PRT(k)} k, i), i = \rho(Pk - \epsilon) \quad (4.21)$$

$$(\rho \epsilon), t + (\rho U i \epsilon - \frac{\rho v_t}{PRT(\epsilon)} \epsilon, i), i = \frac{\rho \epsilon}{k} (C_1 Pk - C_2 \epsilon) \quad (4.22)$$

In this turbulence model,  $\rho$  is the fluid density, and  $v_t$  is the turbulent kinematic viscosity.  $C_\mu$ ,  $C_1$ ,  $C_2$ ,  $PRT(k)$ , and  $PRT(\epsilon)$  is the model constants.  $k$  is the turbulent kinetic energy, determining the energy in turbulence,  $\epsilon$  is the dissipation rate, determining the dissipation rate of turbulent kinetic energy [45]. These factors are presented in Equations 4.23 and 4.24.

$$k = \frac{U_\tau^2}{\sqrt{c_\mu}} \quad (4.23)$$

$$\epsilon = \frac{U_\tau^3}{\kappa d} \quad (4.24)$$

## 4.5 Blockage Effect

The blockage effect reduces the upstream wind speed while extracting energy from a wind turbine or a wind farm [46]. The area around the wind turbine affected by this effect is called the induction zone. The blockage effect in a wind farm leads to less energy production than the initial energy potential [46]. In the simulations in this thesis, the blockage effect is implemented like a refinement type in the Terrain Module in WindSim as a file with blockage at the site included. In wind farm simulation, the blockage effect is often neglected, which can lead to an overprediction of the energy production.

## 4.6 Annual Energy Production (AEP)

In this case, Annual Energy Production (AEP) considers the energy a wind turbine or a wind farm can produce in a year [24]. For wind farm evaluation, AEP is significant for estimating the wind farm quality according to the amount of energy it can produce. The AEP for a wind turbine is calculated by Equation 4.25 [24].

$$AEP = \sum_{j=1}^{N_{tur}} \sum_{i=1}^N P(U_j(x_{turbine,i})) \cdot P_{rated} \cdot \frac{8760h}{N_h} \quad (4.25)$$

Where  $(U_j(x_{turbine,i}))$  is the wind velocity  $i$  at the hub height of wind turbine  $j$ .  $N_h$  is the sample hour,  $N_{tur}$  is the total number of turbines,  $P_{rated}$  is the rated turbine power. The number 8760 h represents the number of hours in a year.

## 4.7 Wind farm capacity factor

The capacity factor of a wind farm describes how much energy it produces compared to the installed wind farm capacity [47]. Therefore, this ratio describes how efficient the wind farm is compared to how much energy that is available in the wind. Equation 4.26 presents the calculation of wind farm capacity factor [48].

$$\eta = \frac{P_T}{P_{in}} = \frac{\frac{AEP/year}{h/year}}{P_{in}} \cdot 100\% \quad (4.26)$$

In this equation,  $P_T$  is the power output, and  $P_{in}$  is the power input, measured in kW. AEP is the annual energy production in kWh/year, and h/year is the number of hours a year, equal to 8760 h.

## 4.8 Wind Speed Distribution

A wind speed distribution is used for wind resource assessment to map the wind potential at a specific site and to further plan, design, construct, and operate a wind farm [49]. Several models for wind speed distribution, with different focus points, have been used for wind farm analysis. The following sections describe the Weibull wind distribution used in this study.

### 4.8.1 Weibull Wind Distribution

The Weibull wind distribution is flexible, simple, and has efficient computing parameters [49]. Therefore, the Weibull distribution is commonly used in various fields, such as physics and material science. In this way, the distribution is known as the most popular wind distribution model. The Weibull distribution is especially advantageous in areas affected by temperate depressions, but the distribution is not as effective at low wind speeds. The Weibull distribution is characterised by two functions describing the variations in wind speed: the Weibull probability density function and the Weibull cumulative distribution function [44]. Equations 4.27 and 4.28 present the probability density and cumulative distribution functions for the Weibull distribution [44].

$$f(V) = \frac{k}{c} \left(\frac{V}{c}\right)^{k-1} \cdot e^{-\left(\frac{V}{c}\right)^k} \quad (4.27)$$

$$F(V) = \int_0^{\alpha} f(V) dV = 1 - e^{-\left(\frac{V}{c}\right)^k} \quad (4.28)$$

In Equations 4.27 and 4.28,  $V$  is the wind speed, and  $k$  and  $c$  are the Weibull shape and scale factor, respectively. Equations 4.29 and 4.30 present the Weibull factors  $k$  and  $c$  [50]. In these equations,  $V_m$  represents the average wind speed and  $\sigma_v$  is the standard deviation.

$$k = \left(\frac{\sigma_v}{V_m}\right)^{-1.090} \quad (4.29)$$

$$c = \frac{2V_m}{\sqrt{\pi}} \quad (4.30)$$

## 4.9 Computational Fluid Dynamics (CFD) analysis

Computational Fluid Dynamics (CFD) is a numerical method for solving fundamental fluid flow equations [51]. The CFD method is useful in several industries, including oil, gas, and automotive. CFD analysis can also be used in renewable energy industries such as wind. In CFD analysis, the Reynolds Averaged Navier-Stokes (RANS) equations describe the fluid flow behaviour, which is time-averaged for the speed fluctuations. The equations are closed by a turbulence model ( $k$ - $\epsilon$ ) in this analysis. Equations 4.31, 4.32, 4.33 and 4.34 present the RANS implemented in this thesis through the simulation in WindSim [52]. In these equations,  $U$  is the wind speed,  $x$  is the positional component,  $P$  is pressure,  $\rho$  is the density,  $\nu$  is the kinematic viscosity,  $\nu_t$  is the turbulent kinematic viscosity, and the subscripts  $i$  and  $j$  are defined unit vectors.

$$\frac{\partial U_i}{\partial x_i} = 0 \quad (4.31)$$

$$U_j \frac{\partial U_i}{\partial x_j} = -\frac{1}{\rho} \frac{\partial P}{\partial x_i} + \frac{\partial}{\partial x_j} \left( \nu \left( \frac{\partial U_i}{\partial x_j} + \frac{\partial U_j}{\partial x_i} \right) - \overline{u_i u_j} \right) \quad (4.32)$$

$$\nu_t = C_\mu \frac{k^2}{\epsilon} \quad (4.33)$$

$$\overline{u_i u_j} = -\nu_T \left( \frac{\partial U_i}{\partial x_j} + \frac{\partial U_j}{\partial x_i} \right) + \frac{2}{3} \delta_{ij} k \quad (4.34)$$

## 4.10 WindSim

WindSim is a Wind Farm Design Tool (WFDT) based on Computational Fluid Dynamics (CFD) [53]. The software can be used for wind farm planning and optimisation to maximise energy production. This procedure is done by locating the areas with the highest wind speeds and considering this in the wind turbine placement. WindSim optimisation happens while keeping the turbine loads under an acceptable limit by calculating numerical wind fields over a digitalised terrain. WindSim covers the whole wind farm lifecycle

through six modules, which include preparatory modules with the implementation of the terrain and wind fields at the wind site and the wind farm design. The last three modules include calculation and simulation of the results for the wind resources and power forecasting. The modelling in WindSim is 3D. This modelling involves wind field characteristics, like wind shear, inflow angle, and turbulence, that affect the loads on the wind turbines [51]. The different modules are described in the sections below.

#### 4.10.1 Terrain module

The Terrain module includes generating a 3D model of the wind site of interest [54]. This 3D model is based on the roughness and elevation data implemented from a file in a .gws format in a regular grid. Equation 4.35 [54] specifies the roughness height in this grid.

$$\frac{U}{U_\tau} = \frac{1}{\kappa \cdot \ln\left(\frac{z}{z_0}\right)} \quad (4.35)$$

In this equation, the wind velocity,  $U$ , is the von Karmans constant equal to 0.435,  $z$  is the coordinate in the vertical direction, and  $z_0$  is the roughness height. The friction velocity  $U_\tau$  is presented in Equation 4.36 including the shear stress  $\tau_0$  and the air density  $\rho$  [54].

$$U_\tau = \left(\frac{\tau_0}{\rho}\right)^{0.5} \quad (4.36)$$

#### 4.10.2 Wind Fields module

The determining of the wind field in the Wind Fields module is based on the 3D model in the Terrain module, in addition to CFD [37]. The generation happens by solving the Reynolds Averaged Navier-Stokes equations (RANS) for an incompressible fluid and applying the turbulence closure, which is the k-epsilon model in this case. The procedure in the Wind Fields module is iterative because of non-linear equations. The wind fields are generated in different wind direction sectors with angles from 0-330° [37].

The RANS Equations in this thesis are presented by Equations 4.31-4.34, which are the ones implemented in WindSim. The RANS equations, in this case, are closed by the standard  $k - \epsilon$  turbulence model for turbulence closure in the simulations and are described by Equations 4.21-4.24 in section 4.4.1 [37].

#### 4.10.3 Objects module

The Object module in WindSim is where the wind farm design process happens. Firstly, the wind site climatology data is imported. With this data, the wind turbine positioning can happen, and the wind farm can be visualised in the 3D terrain model [55]. The placing is done in a coordinate system of choice. The turbine type and parameters like the power curve file (.pws) and turbine size are imported and specified in this process.

#### 4.10.4 Results module

The Results module uses the database from the Wind Fields module and extracts the 2D horizontal planes from this [56]. A normalisation variable has to be implemented, along with the height from which the results should be gathered.

#### 4.10.5 Wind Resources module

The Wind Resources modules give an overview of the wind parameters at the site by weighting the wind database against the climatology [9]. This module provides wind resource maps, including an illustration of the magnitude of the wind speed and a map that forecasts the power production at the site. The Wind Resources module also includes an illustration of the wake for all the wind turbines in the relevant wind farm. Therefore, this model implements a wake model of choice, and the choice is between the three wake models Jensen, Larsen and Ishihara wake models [9].

#### 4.10.6 Energy module

In the Energy module, results like AEP, wake loss and power density for each wind turbine, and the wind farm totals and averages are calculated [57]. Along with these calculations are illustrations of the climatology data, such as wind rose and wind distributions. The results are calculated with the Frequency table and the Weibull wind distribution [57].

### 4.11 WindSim Express

WindSim Express is software for data preparation for WindSim, including creating and converting different WindSim input files. This software allows users to create WindSim power curve files (.pws), including a power curve and a thrust coefficient curve, and object files (.ows) with input details from the desired turbine and the chosen wind farm layout.





## Chapter 5

# Methodology

This chapter includes the study methodology, which involves all the steps in the before, during, and after simulations to gather the results. The following sections include the description of the input data preparation, how the simulations are performed in WindSim, and the method for Project Cases 1 and 2. In addition, information on the wind sites and the turbines used to perform the simulations and gather results is provided.

### 5.1 Preparation of input data

Firstly, the offshore areas up for auction in Norwegian waters were detected in the Norwegian Water Resources and Energy Directorate's identification of Norwegian areas for offshore wind utilisation [5]. Southern Northsea II was chosen as the working area. This choice is based on the technical suitability of the site and because the site is already planned for offshore wind utilisation. The weather data at the site open-meteo.com creates a csv-file that includes significant wind data parameters, like wind speed and direction, by inserting the coordinates of the site. With this data, a WindSim wws-file was made and further used as the climatology data file.

For the turbine, some preparation had to be done to put in the relevant power and thrust data. The power data is gathered from NREL and the NREL page at Git Hub [58] [59]. The thrust data was calculated using Equations 4.17 and 4.18 for the power and thrust coefficient. Further, the power data and thrust coefficient for the different wind speeds were plotted into WindSim Express 10.0 to make the turbine power curve file in a WindSim pws-file format, which includes both the thrust coefficient and power curve.

### 5.2 WindSim

WindSim includes several modules for defining the wind site data and further simulating the production of the wind turbines inserted at the site. The first two modules include the terrain and wind field modules as preparatory modules to define the terrain and wind field data. Further, the Objects module includes the wind farm design process, with the variation of turbine hub heights for some cases. The last three modules are for obtaining results on the wind resources at the site and calculating several wind turbine results, such as the total AEP, wake loss, and power density for each wind turbine and wind farm. The modules are in a

specific order, meaning the first module needs to run correctly for the second to run.

This master's thesis contains an offshore micro-siting approach. The entire procedure will contain several simulations in the different modules in WindSim to include all the necessary parameters for an offshore simulation to be as realistic as possible. The procedures in the different modules are specified in the sections below.

## 5.2.1 Preparatory modules

### Terrain module

The first module in WindSim is the Terrain module. Before this module, while setting up the wind farm project, the grid.gws file is implemented. This file includes the global coordinates of the wind site and terrain information, such as the terrain roughness and information about vegetation, etc. The outcome of the Terrain module is a 3D terrain model containing this information. Since the site is offshore, the variation in roughness at this site is limited.

### Wind Fields module

The site's wind fields are generated in the Wind Fields module. This generation is based on the 3D terrain model from the previous module and determined by resolving the Reynolds Averaged Navier-Stokes (RANS) equations. The standard  $k-\epsilon$  turbulence model is implemented as turbulence closure. The RANS equations are described in Equations 4.31-4.34, and the  $k-\epsilon$  model is described in Equations 4.21-4.24. The wind fields are generated in different wind direction sectors in a uniform distribution of the sector angle, with angles from 0-330°. This wind field generation is an iterative procedure.

### Objects module

After the Wind fields module comes the Objects module. In this module, the climatology is determined by adding the climatology.wws file as a cup anemometer in the Park Layout page of the Object module. Then, a wind turbine with the highest power density was placed at the site area. This design leads to an object.ows file and exporting it to the Terrain module. This file is called object1 and will be used further in simulation.

## 5.2.2 Including actuator discs

For the simulation of an offshore wind farm, actuator discs will be implemented to include the blockage effect so the simulation will be as realistic as possible. From here, four projects are made:

- Project with actuator discs (AD) in a high wind speed regime
- Project with actuator discs (AD) in a low wind speed regime
- Project with high wind speed (no AD)
- Project with low wind speed (no AD)

The AD projects are created by defining the actuator disc as the refinement type in the Terrain module. The other projects use the refinement file from the Terrain module in the AD project as the refinement type and input it as a blockage file. The wind regimes are input in the wind fields module, as the wind speed above the boundary layer is set at 500 m, with a wind speed of 7 m/s representing the low wind speed and 20 m/s representing the high wind speed. The methodology of this part, including actuator discs and blockage effect refinement, is a version of the method from a WindSim workshop about this topic, presented in [60].

### 5.2.3 Wind Farm Design process

The first design process in this study begins with placing 5 MW turbines, one by one, with the starting point of the area with the highest power density at the site and facing the most frequent wind direction. The turbines are placed at a minimum distance of seven times the rotor diameter (7D), with the total annual energy production as the objective function. With this objective function comes the minimisation of the wake losses, and the turbine placement is performed with this in mind. The design process also uses a guidance of approximately 5 MW per square kilometre for offshore wind farms, but it is also set higher to investigate the micro-siting approach. This design process is executed in the Objects module in WindSim, with an evaluation of the AEP and wake loss in the Wind Resources and Energy modules.

The following sections include the methodology for the 5 MW turbine, but the procedure is also adopted for simulation with the 15 MW turbine. The 15 MW turbine characteristics are different from the 5 MW turbine characteristics. The sections about the project cases present a specific description of the simulation methodology in the different cases with the two turbines.

## Results module

Next up is the Results module. This module includes a 3D analysis of the wind speed in the different wind direction sectors. In this module, the wanted property is chosen. In this case, the normalisation variable is the Speed scalar XYZ, and the plane heights for analysis are 70, 90 and 120 m. The 90 m plane is the main plane height since this is the original turbine hub height. These inputs result in visualisation, in the form of figures, of the 3D wind speed in the different wind direction sectors.

## Wind Resources Module

The Wind Resources module includes the implementation of a wake model along with plane heights. In this case, Wake Models 1 and 2, the Jensen and Larsen wake models are implemented in different cases, with the same plane heights in the Results module (70, 90 and 120 m). These implementations lead to several heat maps describing the 2D wind speed, power density, wake deficit, and mean wind speed for the wake deficit at the wind site with the wind farm.

## Energy module

The last WindSim module is the Energy module. This module implements the heights of reference production, the wake model and density correction. In this case, the chosen wake models are numbers 1 and 2, the Jensen and Larsen wake models, and the density correction is pitch-regulated. The multiple wake model is

based on the sum of squares. These inputs result in AEP calculations for the wind farm and each wind turbine in the wind farm, along with other calculations such as wake loss and full load hours. The climatology will also be visualised with a wind rose and probability distributions. These probability distributions are calculated for the Frequency table and Weibull distribution. The Weibull results are used for evaluation in this thesis since it is a commonly used wind distribution.

## 5.3 Project Case 1-Southern Northsea II

Project Case 1 includes three-dimensional micro-siting procedures using the terrain and wind data from the Southern Northsea II wind site. In this project case, two different turbines with different installed capacities, hub heights and sizes are implemented, but the terrain and wind data are the same. The following sections include information on the Southern Northsea II wind site, wind data, and the two turbines used in this project case.

### 5.3.1 Wind resources at Southern Northsea II

The offshore area, Southern Northsea II, is outside the south coast of Norway, and it has been auctioned and planned for offshore wind utilisation. Southern Northsea II has high technical suitability and low conflict of interest for offshore wind [61]. The data for the offshore area is presented in Table 5.1. Figure 5.1 shows the geographical placement of the chosen site, Southern Northsea II. From the newest NVE report on the offshore wind areas in Norway, the Southern Northsea II area is desired to be larger than before, but a part of the original area from 2012, with a size of  $100 \text{ km}^2$ , is used in this study [6].

Table 5.1: Data for Southern Northsea II [6].

Parameter	Magnitude
Size	$2589 \text{ km}^2$
Average wind speed (At 149 m: 15 MW turbine's hub height)	10-10.5 m/s
Significant wave height	2 m
Extreme wave height	11-12 m
Average depth	60 m

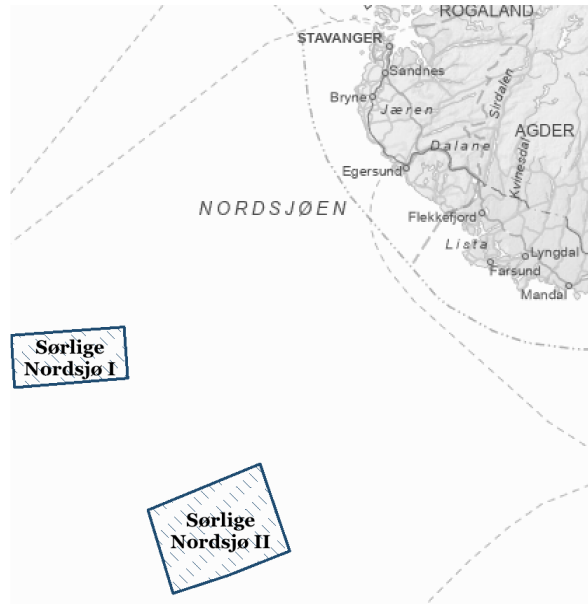


Figure 5.1: Placement of Southern Northsea II on the map.

In Project Case 1, the terrain and wind data from the offshore site at Southern Northsea II are used for simulation. The wind farms are simulated and investigated for layouts with the original turbine hub height and the variation in hub height, which is increased or decreased from the original. Figure 5.2 shows the mean wind speed [m/s] at a 149 m height at the relevant part of the wind site. As described by the spectrum to the left in the figure, the mean wind speed at the site is approximately 10.4 m/s. The part to the lower right of the measurement station is used for all wind farm layouts. This area is  $25 \text{ km}^2$  big. The simulated power density in this part of the Southern Northsea II offshore wind site is shown in the heat map in Figure 5.3. As shown in the spectrum to the left in the figure, the power density at the site varies from 1141.9-1158.4  $\text{W}/\text{m}^2$ . Figures 5.2 and 5.3 are simulated at the original turbine hub height of 149 m since this is the original turbine hub height of the 15 MW turbine.

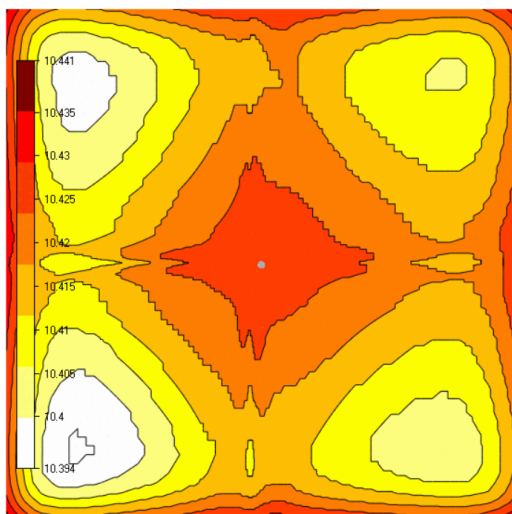


Figure 5.2: The heat map for the wind speeds [m/s] at Southern Northsea II, at a height of 149 m.

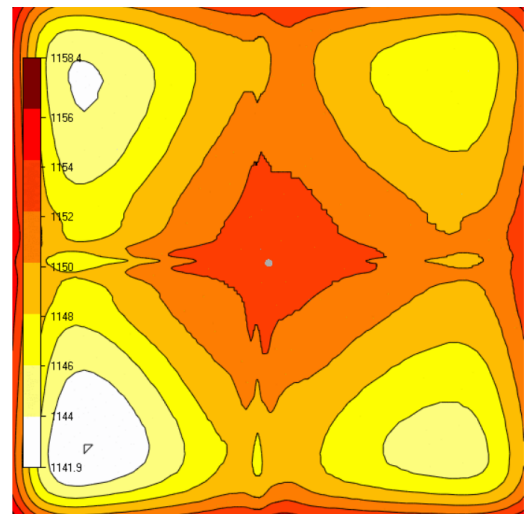


Figure 5.3: The power density [ $\text{W}/\text{m}^2$ ] heat map for the relevant part of Southern Northsea II, at a height of 149 m.

### 5.3.2 Part 1: Wind farms with 5 MW turbines

Part 1 of Project Case 1 includes a three-dimensional micro-siting procedure using NREL's 5 MW reference turbine. Table 5.2 shows the turbine properties of this wind turbine, including the original hub height of 90 m and the rotor diameter of 126 m. Figure 5.4 shows the power and thrust coefficient curve for this wind turbine. The thrust coefficient curve in red increases rapidly at a wind speed of approximately 2.5 m/s, is stable around 0.88 from 3-7 m/s and decreases evenly after 7 m/s before it evens out at around 25 m/s. The black power curve increases evenly at approximately 3 m/s, peaks at 15 m/s, and maintains stability before decreasing slowly from 19 m/s.

Table 5.2: Pre-set properties for the 5 MW NREL Baseline Wind Turbine [62].

Property	Magnitude
Rating	5 MW
Rotor Orientation, Configuration	Upwind, 3 Blades
Control	Variable Speed, Collective Pitch
Drivetrain	High Speed, Multiple-Stage Gearbox
Rotor, Hub Diameter	126 m, 3 m
Hub Height	90 m
Cut-In, Rated, Cut-Out Wind Speed	3 m/s, 11.4 m/s, 25 m/s,
Rated Tip Speed	80 m/s

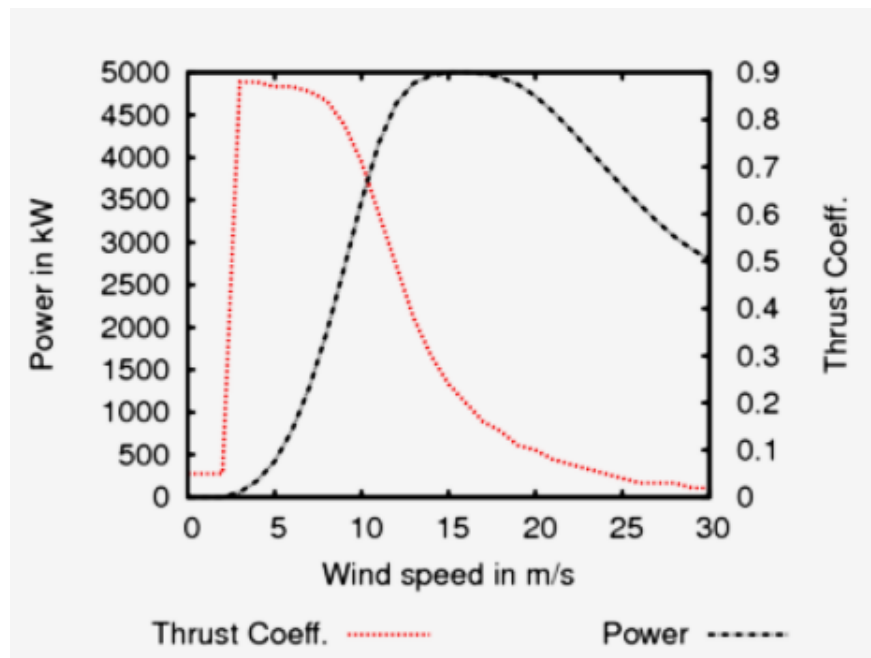


Figure 5.4: The power and thrust coefficient curve for the 5 MW NREL reference turbine.

### Three-dimensional micro-siting approach

This three-dimensional micro-siting approach includes wind farm simulation with a certain capacity density, including 5 MW turbines with the original hub height of 90 m. Firstly, a wind farm with a  $5.4 \text{ MW}/\text{km}^2$  capacity density is designed at a  $25 \text{ km}^2$  area at the wind site, Southern Northsea II. This capacity density is a guidance value for offshore wind farms. Further, a version of this layout was made by varying the turbines' hub height, ranging from 80 to 120 m. This procedure happens by changing the hub height of the turbines, one by one, in the Objects module in WindSim. The AEP and wake loss are evaluated after every hub height variation to see if the results improved and decide which turbine to change next. This procedure was performed until the AEP did not increase further, and the wake loss did not decrease, indicating satisfaction with the results. The described approach was performed for capacity densities between  $5.4\text{-}8 \text{ MW}/\text{km}^2$ . The capacity density is increasing by adding more 5 MW turbines to the  $25 \text{ km}^2$  area. Figure 5.5 is an example of a wind farm layout with 5 MW turbines, included in the study. This layout has a  $6 \text{ MW}/\text{km}^2$  capacity density, including 30 turbines of 5 MW, with a minimum turbine distance of approximately 7D.



Figure 5.5: The  $6 \text{ MW}/\text{km}^2$  capacity density wind farm with 30 turbines of 5 MW.

#### 5.3.3 Part 2: Wind farms with 15 MW turbines

Part 2 of Project Case 1 also includes the wind data from Southern Northsea II and follows the procedure in Part 1. However, the difference is that this part uses the NREL's 15 MW reference turbine. The NREL 15 MW reference turbine properties are presented in Table 5.3. This turbine has an original rotor diameter of 248 m and a hub height of 149 m. The table shows that this turbine has a cut-in wind speed of 4 m/s and is rated at 11 m/s. The cut-out wind speed is 25 m/s, a typical value for wind turbines. Figure 5.6 presents the power and thrust coefficient curve for the NREL 15 MW reference turbine created in WindSim Express. The power curve increases from 0-15000 kW in the wind speed range of 4-11 m/s and is kept stable at 15000 kW until the cut-out wind speed, which is 25 m/s. The thrust coefficient curve increases drastically from 0 to approximately 0.89 between 3-7 m/s and is stable before it decreases evenly at 12 m/s and decreases drastically to 0 at the cut-out wind speed.

Table 5.3: Pre-set properties for the 15 MW NREL Baseline Wind Turbine [58].

Property	Magnitude
Rating	15 MW
Rotor Orientation, Configuration	Upwind, 3 Blades
Control	Variable Speed, Pitch regulated
Drivetrain	Direct drive
Rotor Diameter	248 m
Hub Height	149 m
Cut-In, Rated, Cut-Out Wind Speed	4 m/s, 11 m/s, 25 m/s

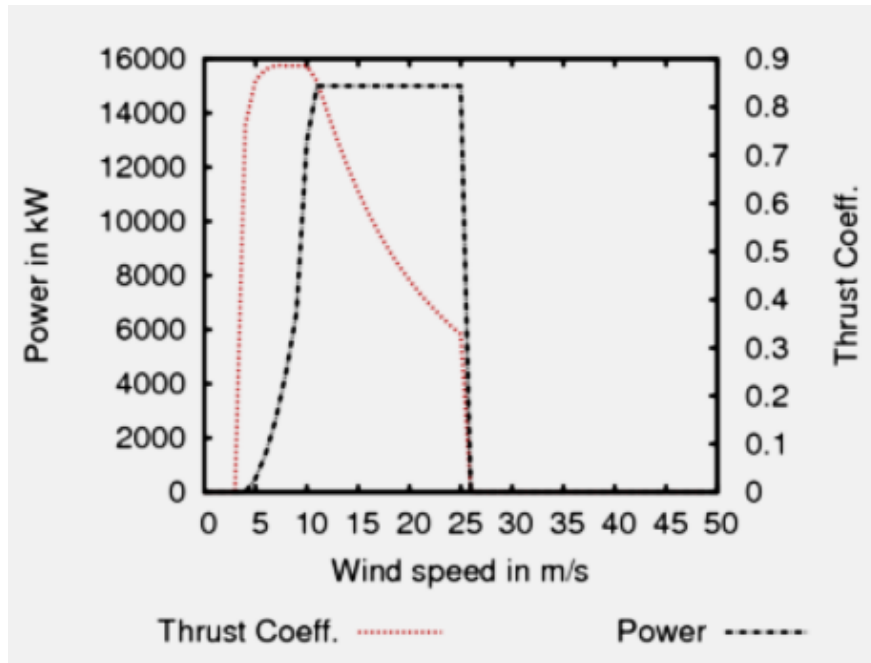


Figure 5.6: The power and thrust coefficient curve for the 15 MW NREL reference turbine.

### Three-dimensional micro-siting approach

The three-dimensional micro-siting is performed from the capacity density starting point of  $5.4 \text{ MW}/\text{km}^2$ , including the 15 MW turbine with a 149 m hub height. From this layout, a new layout is created with the turbine hub heights varied one by one in a range of 135–179 m. Between every variation is an evaluation of the AEP and wake loss, and the hub height variation happens until satisfaction. Further, this procedure was performed for wind farms with capacity density between  $6\text{--}15 \text{ MW}/\text{km}^2$  in the  $25 \text{ km}^2$  area. Figure 5.7 shows an example of a wind farm layout with the 15 MW turbine. This layout contains nine turbines, constituting a wind farm capacity density of  $5.4 \text{ MW}/\text{km}^2$  and a 7D distance between the turbines.



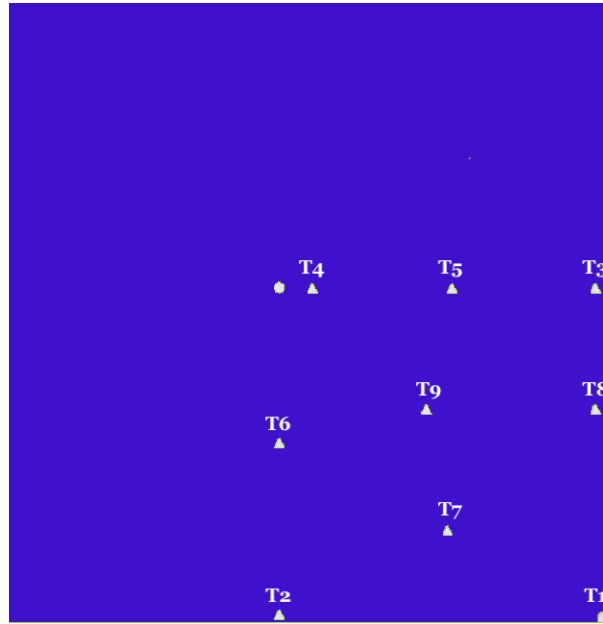


Figure 5.7: The  $5.4 \text{ MW}/\text{km}^2$  wind farm layout with 9 turbines of 15 MW.

## 5.4 Project Case 2-Virtual wind farms

In addition to Project Case 1 at Southern Northsea II, Project Case 2, a virtual wind farm case, is performed to investigate the impact of three-dimensional micro-siting at a site with lower wind speeds and different wind conditions. The project case is virtual since the geographical site of Southern Northsea II is used, together with the wind data from the Smøla wind site. Project Case 2 uses the 15 MW turbine and is performed in the same way as the second part of Project Case 1. Firstly, the wind farm layouts are designed with an original turbine hub height of 149 m for different capacity densities. Then, the turbine hub heights are varied, with heights ranging from 135 to 179 m. This procedure is done for capacity densities from 6-15  $\text{MW}/\text{km}^2$ . The wind conditions at the site are described in the following section.

### 5.4.1 Wind resources at Smøla wind site

Project Case 2 includes the same offshore site as in Project Case 1 with the 15 MW turbine, but the wind data is gathered from Smøla in northwestern Norway, an onshore wind site. This wind data generally has lower wind speeds than the original at Southern Northsea II and has different frequencies in the wind directions. Figures 5.8 and 5.9 show the heat maps for mean wind speeds and power density for the wind site in Project Case 2, including the blockage refinements. Figure 5.8 shows that the mean wind speed at this site is approximately 7.7 m/s. This wind speed is 2-3 m/s lower than the mean wind speed in Project Case 1. The wind speed in Project Case 2 is strongest in places with the darkest colours, which are around the edges and in the centre of Figure 5.8. The spectrum to the left in Figure 5.9 shows that the power density at the site is originally between 686-700  $\text{W}/\text{m}^2$ . Figures 5.8 and 5.9 are simulated at the original turbine hub height of 149 m.

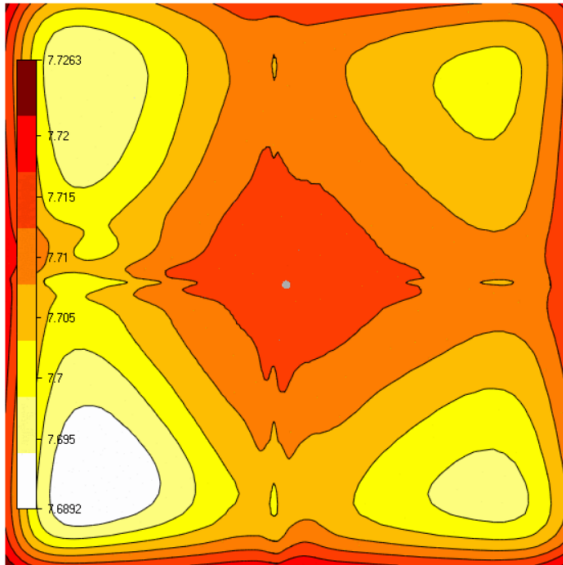


Figure 5.8: The heat map for the wind speeds [m/s] in Project Case 2 at a height of 149 m.

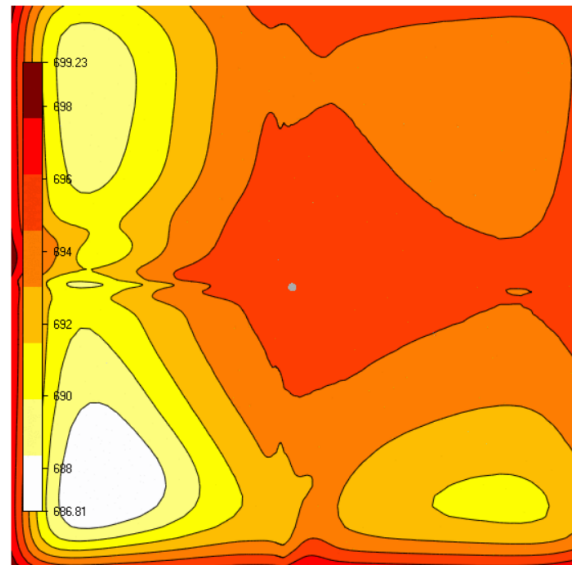


Figure 5.9: The power density [ $W/m^2$ ] heat map for the site in Project Case 2 at a height of 149 m.

### 5.4.2 The Project Cases

Table 5.4 is an overview of the different project cases in this thesis. The table includes information about the turbine, wind resources and wake models used in the different project cases. All project cases used the same wake models, but the turbine and wind resources could vary.

Table 5.4: Description of the different project cases.

Project Case	Turbine	Wind resource	Wake model
Project Case 1, part 1	5 MW	Southern Northsea II (Mean: 10.4 m/s)	Models 1 and 2
Project Case 1, part 2	15 MW	Southern Northsea II (Mean: 10.4 m/s)	Models 1 and 2
Project Case 2	15 MW	Smøla wind site (Mean: 7.7 m/s)	Models 1 and 2

## 5.5 Computational parameters

Table 5.5 presents some of the input parameters in WindSim. These parameters are put in the different modules in WindSim and chosen as best for the site criteria. For example, the number of iterations is chosen because of the computational time for the simulation. For the area size in WindSim, a  $100 \text{ km}^2$  big area is the starting point, but to decrease the total number of turbines, a quarter of this area is used, which means  $25 \text{ km}^2$ . In addition to WindSim and WindSim Express, Excel has been used to sort the results and perform calculations, and Python has been used to plot the graphs in this study. In the writing process, the Grammarly app was used to correct the spelling of words and grammar in the sentences.

Table 5.5: Input parameters in WindSim.

Category	Value
X-range (UTM coordinates)	428436.443; 438436.443
Y-range (UTM coordinates)	490220.208; 500220.208
Refinement	Refinement file from project with AD
Turbulence model	Standard k- $\epsilon$
Number of iterations	70
Normalisation variable	Speed scalar XYZ
Wake models	Wake models 1 and 2: the Jensen and Larsen wake models



## Chapter 6

# Results and Discussions

This chapter presents the results and discussions of this thesis, including the three-dimensional micro-siting approach through wind farm simulation in WindSim. These simulations encompass several project cases to investigate the procedure of three-dimensional micro-siting using different wind data, turbines, and wake models. The wind farms featuring 5 MW and 15 MW turbines are created to investigate the approach, including different capacity densities and wake models. The wake models included are Wake Models 1 and 2, which represent the Jensen and the Larsen wake models, respectively.

Performance of the three-dimensional wind farms with turbines of 5MW and 15 MW rated capacities are being analysed at capacity densities ranging from 5.4 to 15  $MW/km^2$ . Both wind turbines considered are the National Renewable Energy Laboratory (NREL) reference turbines. The following sections present the results from these simulations.

### 6.1 Southern Northsea II

Project Case 1 in this thesis includes terrain and wind data from the Southern Northsea II area. The wind data for the site is illustrated by the wind rose in Figure 6.1 and the wind speed distributions in Figure 6.2. The wind rose includes the site's different wind speeds, direction, and frequency of the wind speeds in the different wind directions. The figure shows that the wind direction is most frequent for the angles between approximately 190-350°. As mentioned earlier, the mean speed at the site is 10.4 m/s, but the wind rose shows that this value is often exceeded. The darker colours in the figure indicate the higher wind speeds, which occur a considerable amount of the time in the Southern Northsea II area.

Figure 6.2 indicates the Weibull distribution of wind at Southern Northsea II depicted by the red, dotted line. The figure also includes the actual data represented by the bars. The Weibull distribution fitted over the actual data closely aligns with the real observations collected from the wind site. This analysis shows that the most probable wind speed at the site is 11 m/s, 10 m/s for the Weibull distribution, and the chances of extreme wind speeds above 25 m/s are very rare.

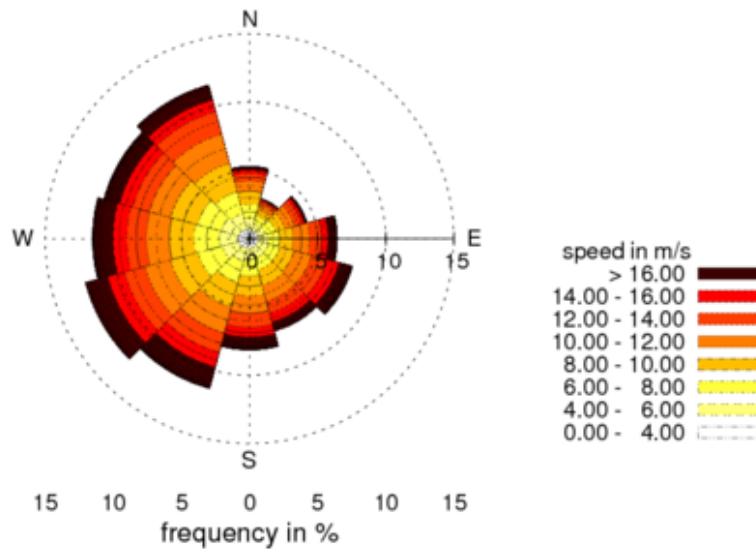


Figure 6.1: The wind rose for the Southern Northsea II wind site, used in Project Case 1.

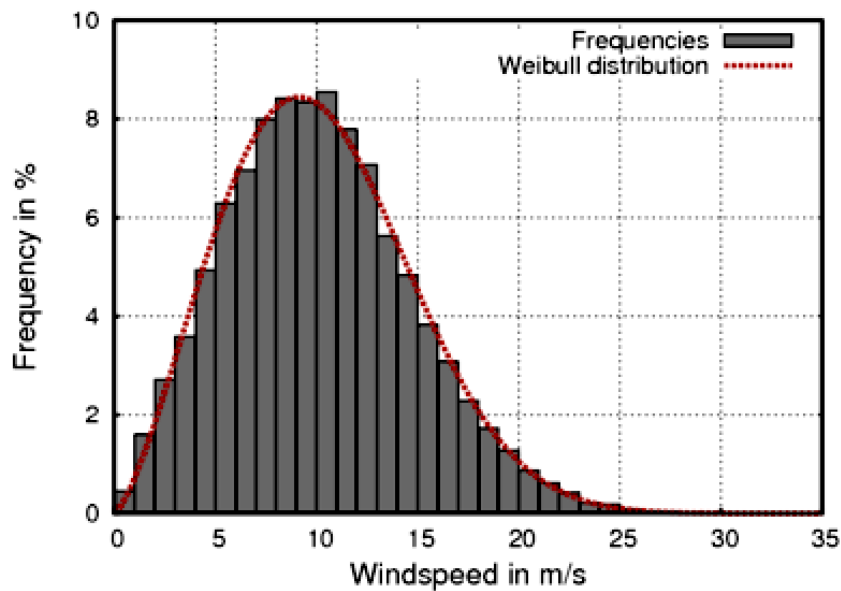


Figure 6.2: The Weibull distribution of wind (red line) fitted over the actual wind data (grey bars) at Southern Northsea II, used in Project Case 1.

## 6.2 Onshore wind site at Smøla

Project Case 2 of this thesis includes implementing the wind data from an onshore wind site at Smøla. Figure 6.3 presents the wind rose in this virtual project, including the wind speeds and wind directions at the site. The wind rose in the figure shows that the wind speeds at the Smøla wind site are primarily between 4-10 m/s. Furthermore, the most frequent wind direction is clearly in a west-southern direction, indicating a direction of approximately 240-260°, with a frequency of approximately 18%. The wind direction also includes high wind speeds.

Figure 6.4 presents the Weibull distribution of wind at the Smøla wind site. In this figure, the red line

representing the Weibull distribution is fitted to the bars, representing the site's actual wind data. The actual data indicates that the most probable wind speed at the site is 5 m/s. For the Weibull distribution, the most probable wind speed is 4 m/s. The analysis shows that the Weibull wind distribution is not as aligned with the actual data as desired for the lower wind speeds, which confirms the weakness of the distribution at lower wind speeds. But the most probable wind speed is almost the same. This analysis also shows that the chances of extreme wind speeds over 25 m/s are rare.

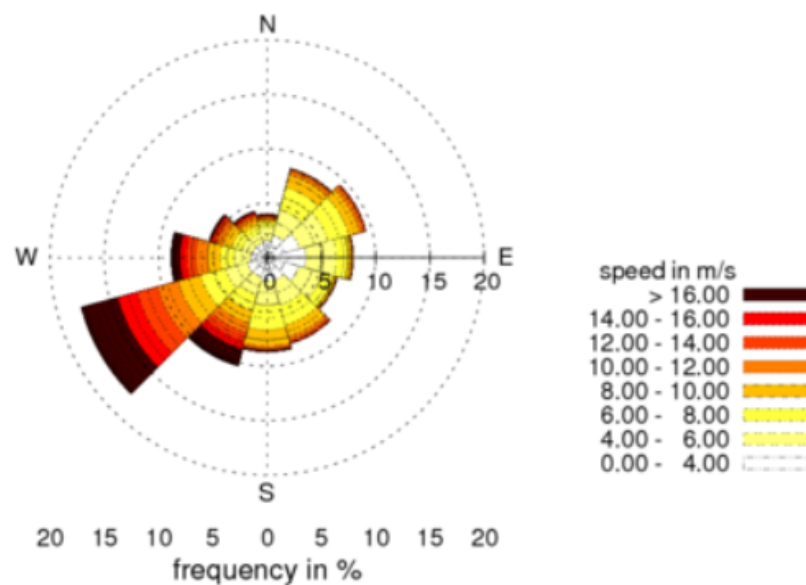


Figure 6.3: The wind rose for the Smøla wind site used in Project Case 2.

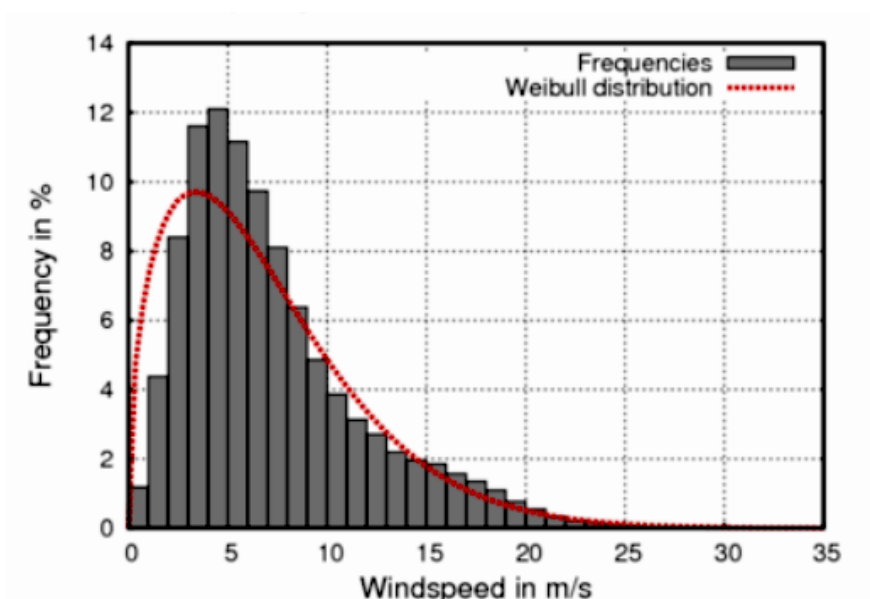


Figure 6.4: The Weibull distribution of wind (red line) fitted over the actual wind data (grey bars) at Smøla wind site, used in Project Case 2.

## 6.3 Three-dimensional micro-siting with 5 MW turbines

The next sections present the results for the wind farm layouts with the 5 MW turbine. The 5 MW turbine is only implemented in Project Case 1. The results include the estimated total AEP, capacity factor, and wake loss with the two wake models at different capacity densities. The exact estimated values for wind farm AEP, capacity factors, and wake loss are presented in Appendix A.

### 6.3.1 Project Case 1: Part 1

#### Annual Energy Production (AEP) evaluation

Figure 6.5 shows the estimated annual energy production (AEP) at different capacity densities for the original (2D) and varying (3D) hub height wind farms in the first part of Project Case 1. The figure includes the results for both Wake Models 1 and 2. Analysis of the figure indicates a linear increase of AEP as the number of turbines and the capacity density increase for the implemented scenarios. The analysis of the AEP also indicates that the AEP of the wind farms with 3D siting is higher than the conventional 2D siting in the case of all the capacity densities with both wake models. The difference between the 2D and 3D AEP increases as the capacity density increases. With Wake Model 1 implemented, the AEP increases by 7743.6-13989.4 MWh/y for the included capacity densities: 5.4-8 MW/km<sup>2</sup>. Similarly, the AEP with Wake Model 2 increases by 7866.4-14772.2 MWh/y in the same case.

In this project case, implementing the variable height concept does not seem to result in a significant enhancement in the AEP of the wind farms. The reason for this can be that the wind site used in this project case has a relatively strong wind spectrum, with a mean wind speed of 10.4 m/s. By analysing the cumulative distribution of wind at the site, a considerable amount of the time, the wind speed is above the

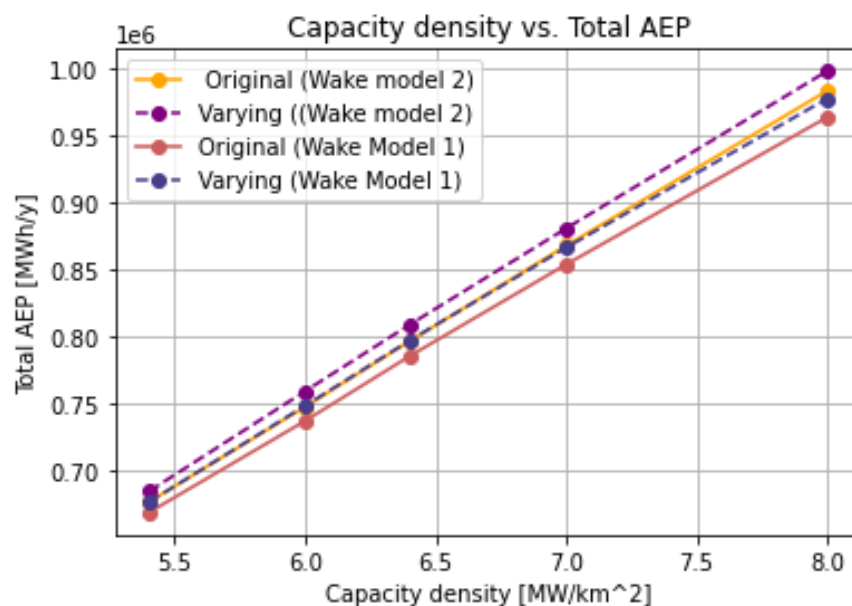


Figure 6.5: The total AEP [MWh/y] at different capacity densities for the first part of Project Case 1. Both Wake Models 1 and 2 are included in the figure.



rated wind speed of the turbine. Hence, any reduction in the wake losses will, therefore, not be reflected in the AEP because the turbine already works in the rated wind speed region. However, the AEP will increase as the capacity density is improved.

### Capacity factor evaluation

Figure 6.6 presents the capacity factor for the capacity densities between 5.4-8  $MW/km^2$  in Project Case 1 with 5 MW turbines. The estimated capacity factors with Wake Models 1 and 2 are presented in the figure, including the original and varying hub height scenarios. The figure shows that the capacity factor decreases as the capacity density increases for all scenarios since the number of turbines increases; therefore, more energy loss is naturally considered. Analysis with Wake Model 1 indicate that the capacity factor increases by 0.65-0.87 % for all capacity densities by varying the turbine hub heights. With Wake Model 2, the capacity factor increases by 0.67-0.89 % for all capacity densities in the same scenario.

The figure indicates significantly higher capacity factors with Wake Model 2 than with Wake Model 1. The impact of the variable hub height concept is also greater in the Wake Model 2 scenario. As the capacity density exceeds 6  $MW/km^2$ , analysis with Wake Model 1 indicates a steeper decrease than with Wake Model 2, which decreases less in this area.

The findings with Wake model 1 indicate that the wind farm capacity density can be increased from 5.4-7  $MW/km^2$  by varying the turbine hub heights. This way, the capacity factor of 56.5 % at this point is maintained, but the wind farm can gather a better energy output. Analysis with Wake Model 2 indicates that the capacity density can be increased from 5.7-8  $MW/km^2$  and still have the same capacity factor by varying the turbine hub heights. But in this scenario, the capacity factor is 0.5 % higher than for Wake Model 1, indicating a capacity factor of 57 %. The difference between the capacity factors for the 2D and

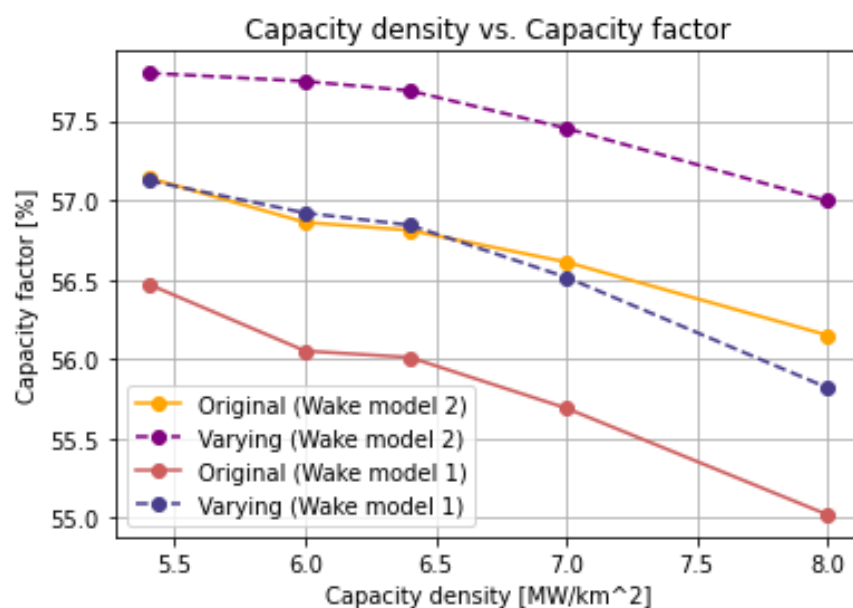


Figure 6.6: The capacity factor [%] at different capacity densities for the first part of Project Case 1. Both Wake Models 1 and 2 are included in the figure.

3D micro-siting in these scenarios with 5 MW turbines is marked, meaning that the turbines can be closer, and the capacity factor can stay the same, including an increase in the AEP.

Even though the capacity factor increases by varying the turbine hub height, the increase is under 1 % for both wake scenarios. As previously mentioned, this can be due to the wind turbine’s rated wind speed being close to the most frequent wind speed at the wind site, including the wind speeds being over the rated wind speed in a considerable amount of time. This similarity can affect the capacity factor change and prevent significant increases by implementing the 3D micro-siting approach in wind farms.

### Wake loss evaluation

Figure 6.7 shows the wake loss for capacity densities between 5.4-8  $MW/km^2$  in the first part of Project Case 1. The figure includes original and varying hub height layouts and both Wake Models 1 and 2. Analysis of wake loss with both wake models indicates that the wake loss increases as the capacity density and the number of turbines increase. By hub height variation, the wake loss with Wake model 1 decreases by 0.31-0.46 % for the implemented capacity densities. With Wake model 2, the wake loss decreases by 0.32-0.52 % by varying turbine hub height for the same capacity densities. In both wake scenarios, the hub height variation positively impacts the wake losses, including a more significant decrease as the capacity density increases.

In this project case, the wake loss is significantly higher for the original and varying hub height scenarios with Wake model 1 implemented than with Wake model 2. Similarly to the capacity factors in this case, the variable hub height concept has a greater impact on the wake loss with Wake Model 2 than on the wake loss with Wake Model 1. This includes a more significant decrease in the wake losses by hub height variation with Wake Model 2 compared to Wake Model 1 for all capacity densities.

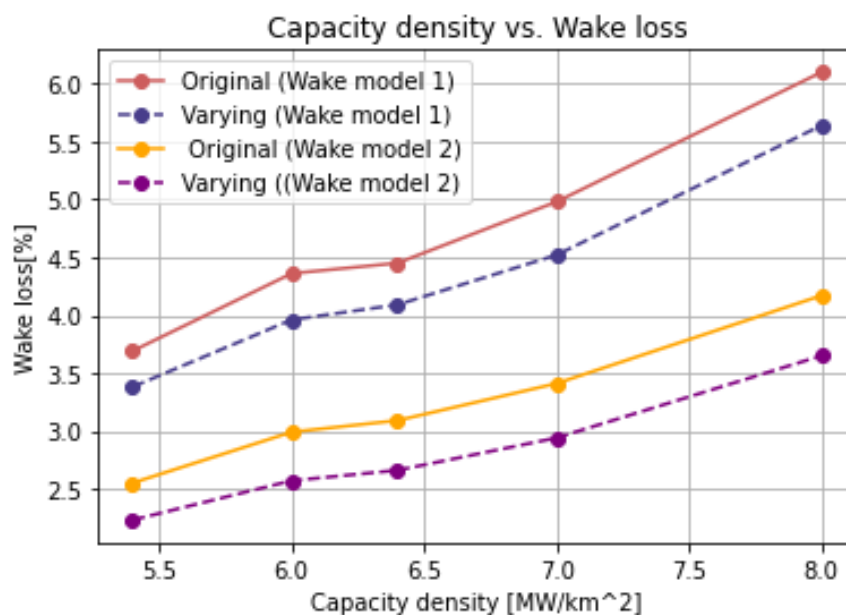


Figure 6.7: The wake loss [%] at different capacity densities for the first part of Project Case 1. Both Wake Models 1 and 2 are included in the figure.

The analysis of the wake losses in this project case indicates a possibility for an increase in the capacity density of a wind farm, including maintenance of the wake loss by including the variable hub height concept. For the scenario with Wake Model 1, this can concern a capacity density increase from  $6.4 \text{ MW}/\text{km}^2$  to  $7 \text{ MW}/\text{km}^2$  capacity and maintaining the wake loss of 4.5 %. For this scenario with Wake model 2, the capacity density can increase from  $6 \text{ MW}/\text{km}^2$  to  $7 \text{ MW}/\text{km}^2$ , and the original wake loss of 3 % can be maintained. These results indicate that the turbine spacing can be decreased from the included minimum distance of 7D by implementing the variable hub height concept according to the wake loss.

## 6.4 Three-dimensional micro-siting with 15 MW turbines

The sections below present the results for the wind farm layouts with the 15 MW turbine. This 15 MW turbine is implemented in both Project Cases 1 and 2, including wind farms with original and varying turbine hub heights. The project cases are conducted with two different wake models for wake simulation, Wake Model 1 and 2, which correspond to the Jensen and the Larsen wake models.

### 6.4.1 Project Case 1: Part 2

The results from the second part of Project Case 1, including the 15 MW turbine, are shown in the sections below. The objectives in the project case are the total AEP, capacity factor, and wake loss for different capacity densities, including the two different wake models. The exact numbers for AEP, capacity factors, and wake loss are presented in Appendix B.

#### Annual Energy Production (AEP) evaluation

Figure 6.8 shows the total AEP for Project Case 1 with 15 MW turbines, including original and varying hub heights. Wake Models 1 and 2 are implemented in this figure for capacity densities between  $5.4\text{-}15 \text{ MW}/\text{km}^2$ . The analysis with Wake Model 1 indicates that the total AEP with Wake Model 1 for original and varying hub heights are similar at the start and separate as the capacity density exceeds  $10 \text{ MW}/\text{km}^2$ . From  $10.2\text{-}15 \text{ MW}/\text{km}^2$ , the AEP increases by  $7768.5\text{-}14664.8 \text{ MWh}/\text{y}$  with Wake Model 1 due to hub height variation. The analysis with Wake Model 2 indicates that the AEP has no significant increase by hub height variation for the capacity density between  $5.4\text{-}10 \text{ MW}/\text{km}^2$ . As the capacity density increases, the hub height variation impacts the AEP more, including an increase of  $9605.2\text{-}17884.7 \text{ MWh}/\text{y}$  for the capacity densities between  $10.2\text{-}15 \text{ MW}/\text{km}^2$ .

Analysis of the figure, including the two wake models, indicates that for the lower capacity densities ( $5.4\text{-}10 \text{ MW}/\text{km}^2$ ), the AEP have no significant difference between the wake scenarios. As the capacity density and the AEP increase, the difference between the wake scenarios also increases. The analysis of the two wake models indicates higher AEP with Wake Model 2, with a more significant difference as the capacity density increases.

In this project case, the implementation of variable hub heights did not indicate a significant enhancement of the AEP of the wind farms with the two wake models. However, the AEP increases with the increasing

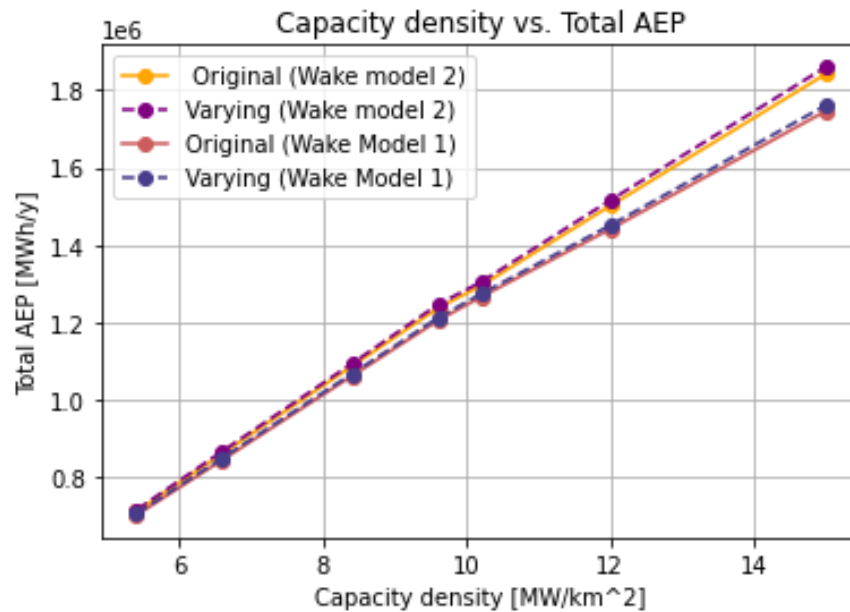


Figure 6.8: The total AEP [MWh/y] at different capacity densities for the second part of Project Case 1. Both Wake Models 1 and 2 are included in the figure.

capacity density for both wake scenarios. By increasing the turbine hub heights, the wind turbines will catch higher wind speeds as the higher wind fields hold higher wind speeds. In this way, the AEP naturally increase with variable hub heights without the wake loss, and prospective wake loss decreases, constituting much.

### Capacity factor evaluation

The capacity factor is plotted against the capacity density for Project Case 1 with the 15 MW turbine in Figure 6.9. The figure shows the capacity factors for the original and varying hub height wind farms, including Wake Models 1 and 2. Both scenarios are performed with wind farms with capacity densities between 5.4-15  $MW/km^2$ . In the figure, the capacity factor decreases as the capacity density increases for the implemented scenarios. Analysis with the two wake models indicates a capacity factor increase of 0.3-0.45 % and 0.33-0.54 %, respectively, by including 3D micro-siting to the wind farms with Wake Model 1 and 2.

The capacity factors gathered by Wake model 2 implementation are significantly higher than for Wake model 1. After the 10.2  $MW/km^2$  capacity density, the capacity factor drops significantly for both Wake model 1 scenarios. This drop leads to a more significant difference between the capacity factors of the two wake models as the capacity density increases above 10.2  $MW/km^2$ . The Wake model 2 capacity factors drop for capacity densities between 9.6-10.2  $MW/km^2$  but stabilise slightly as the capacity density increases further. The effect of hub height variation is also more significant for the Wake model 2 scenarios, meaning that the capacity factor increases more by varying the hub heights for the Wake model 2 scenarios than the Wake model 1 scenarios. The dropping capacity factors for Wake Model 1 at higher capacity densities can be due to the simplicity of Wake Model 1. The simplicity makes the wake model more accurate in far-wake regions than near-wake regions. For the higher capacity densities, the turbines are placed much closer than lower capacity

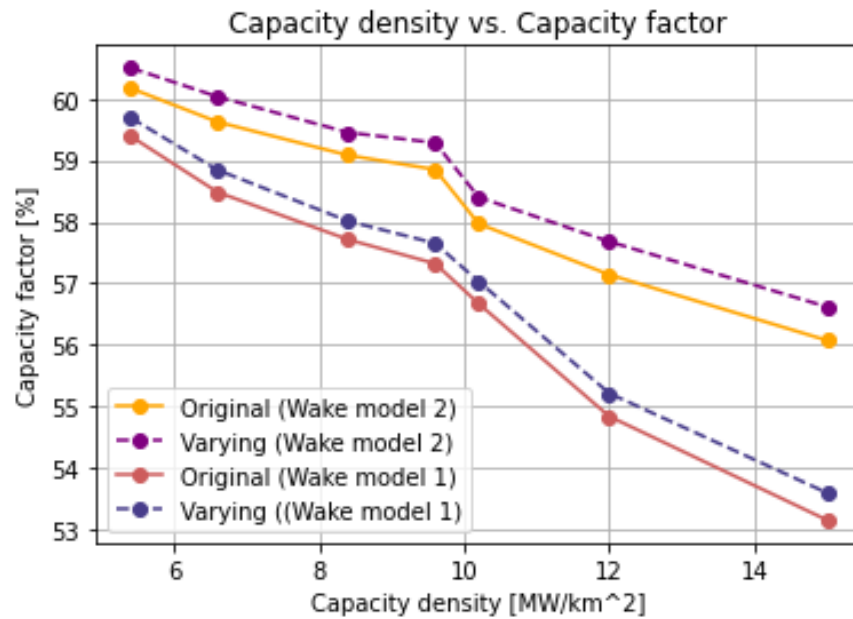


Figure 6.9: The capacity factor [%] at different capacity densities for the second part of Project Case 1. Both Wake Model 1 and 2 are included in the figure.

densities with a minimum distance of 4D-5D, which can be identified as the near-wake region. Wake Model 2 is a more complex model, which can cause more stabilised capacity factors as the turbine spacing decreases.

For the original  $6.6 \text{ MW}/\text{km}^2$  capacity density layout with Wake Model 2, the capacity factor is 59.62 %. This capacity factor is also gathered by a layout of approximately  $8 \text{ MW}/\text{km}^2$  in capacity density with hub height variation. This result indicates that in this case, the wind farm capacity density can increase by  $1.4 \text{ MW}/\text{km}^2$  with varying the turbine hub heights, including reduction of the turbine distances from a minimum of 7D to approximately 6D. The turbines will, therefore, be significantly closer to each other, with the same wind farm capacity factor but higher capacity density. These factors make it possible to add more turbines to the wind farm and, therefore, increase the installed capacity and energy production. For the same case with Wake Model 1, the capacity density could have increased by  $1.4 \text{ MW}/\text{km}^2$ , and the capacity factor would have stayed the same. However, this capacity factor is lower than for Wake Model 2 and, therefore, equal to 58.84 %.

### Wake loss evaluation

Figure 6.10 shows the wake losses for each wind farm capacity density in Project Case 1 with the 15 MW turbine. The figure includes the wake loss for the original and varying hub height layout with both Wake Models 1 and 2. For all scenarios, the wake losses increase as the capacity density increases. Analysis of wake loss with Wake Model 1 for original and varying hub heights shows that the wake loss is not significantly enhanced by hub height variation for the lower capacity densities. As the capacity density increases to 12 and  $15 \text{ MW}/\text{km}^2$ , the original wake loss drastically increases from the previous capacity densities. Therefore, there is also a more significant decrease in wake loss by varying the hub heights in the wind farms with 0.11 % and 0.32 % decrease for the  $12 \text{ MW}/\text{km}^2$  and  $15 \text{ MW}/\text{km}^2$ . For Wake Model 2 analysis, the wake losses

decrease by hub height variation is not significant for the capacity densities between 5.4-10.2  $MW/km^2$ . As for Wake Model 1, the wake loss increases as the capacity density increases in both the original and varying hub height scenarios. As the capacity density exceeds 11  $MW/km^2$ , the wake loss decreases by variation in hub heights is more considerable, including a decrease of 0.36-0.47 %. These results indicate that the 3D micro-siting approach is more beneficial for higher capacity densities for both wake models.

The wake loss with Wake Model 2 is significantly lower than Wake Model 1, and the difference between them increases as the capacity density increases. For the Wake Model 2 scenarios, the decrease in wake loss between the original and varying hub height is more significant than for Wake Model 1. With both wake models, the wake loss decrease is small for capacity densities lower than 10  $MW/km^2$ , including differences of less than 0.2 %. As the capacity density exceeds 10  $MW/km^2$ , the wake loss increases more than before, but the increase is more drastic for the Wake model 1 case than for Wake model 2. The Wake Model 2 wake loss almost stabilises as the capacity density increases.

As in the first part of Project Case 1, the implemented wind regime is a wind regime with relatively high wind speed, including a mean of 10.4 m/s. The cumulative distribution of the site also indicates that for a considerable amount of time, the wind speed exceeds the wind turbine’s rated wind speed. The prospective wake loss reduction may not be reflected in the results, as the turbine already works at the wind speed it is controlled to work at.

Although the wake losses, in this case, do not decrease much by varying turbine hub heights, there is no significant increase in the original wake loss for the lower capacity densities. As mentioned, the capacity density can be increased with the benefits of a better AEP and keeping the capacity factor. Therefore, this capacity density increase can happen without the wake losses increasing significantly, and overall, the wind

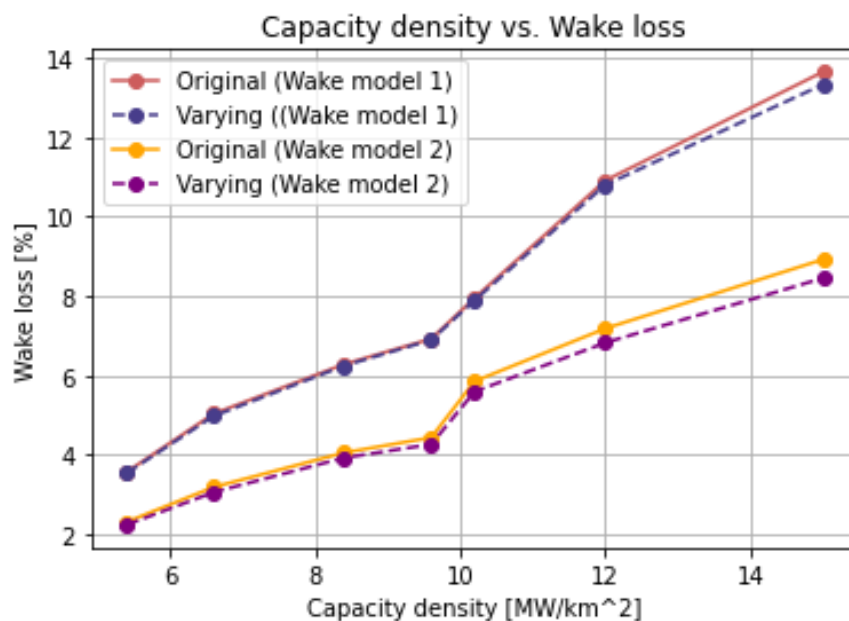


Figure 6.10: The wake loss [%] at different capacity densities for the second part of Project Case 1. Both Wake Models 1 and 2 are included in the figure.

farm layout may benefit from a capacity density increase for both wake models in this case.

The total wind farm AEP in Project Case 1, with 15 MW turbines, does not significantly increase by varying the turbine hub heights. In addition, the decrease in wake loss is small for both wake model cases. By implementing the 3D micro-siting approach, the AEP will increase automatically without the wake loss counting much. This automatic increase is due to higher wind speeds at higher wind fields, which leads to an automatic increase in AEP. These results indicate that the wake loss decrease due to hub height variation may not count much in this case, and the increase in AEP can result from the turbines catching higher wind speeds. However, the capacity factor only decreases slightly for lower capacity densities. The wake losses barely increase for the same capacity densities, leading to the possibility of increasing the capacity density by varying the hub heights, and the AEP can increase. In addition, the wind speeds at Southern Northsea II often exceed the turbine's rated wind speed. This aspect can affect the effect of hub height variation in a wind farm.

### 6.4.2 Project Case 2

The following sections present the results from Project Case 2. These results focus on total wind farm AEP, wake loss and capacity factor. The exact values for these parameters are presented in tables in Appendix C.

#### Annual Energy Production (AEP) evaluation

Figure 6.11 shows the total AEP for Project Case 2, including the simulation results with the two different wake models, Wake models 1 and 2. The figure includes capacity densities between 6-15  $MW/km^2$ . The AEP with Wake Models 1 and 2 indicates no significant increase by implementing the variable hub height concept. The analysis with Wake Model 1 indicates an AEP increase of 4000-6400 MWh/y for the capacity densities below 10.2  $MW/km^2$  by varying the hub heights. However, the impact of the hub height variation is more pronounced for the higher capacity densities, resulting in an increase of 11020.8 MWh/y for the 15  $MW/km^2$  layout. For the Wake Model 2 wind farms, the figure indicates an AEP increase of 4800-8700 MWh/y for the capacity densities under 10  $MW/km^2$  by including hub height variation. However, with Wake Model 2, the impact of the approach also increases with the increasing capacity density, indicating an increase of 14316.5 MWh/y in AEP for layout with 15  $MW/km^2$  capacity density.

The AEP in the two wake scenarios are similar initially, but as the capacity density increases, the estimated AEP with Wake Model 2 increases from the Wake Model 1. The gap between the results is biggest at the highest capacity density: 15  $MW/km^2$ . The AEP increases because of hub height variation in both wake scenarios, but the increase is not significant. However, the AEP naturally increases as the capacity density increases, and the increase is close to linear.



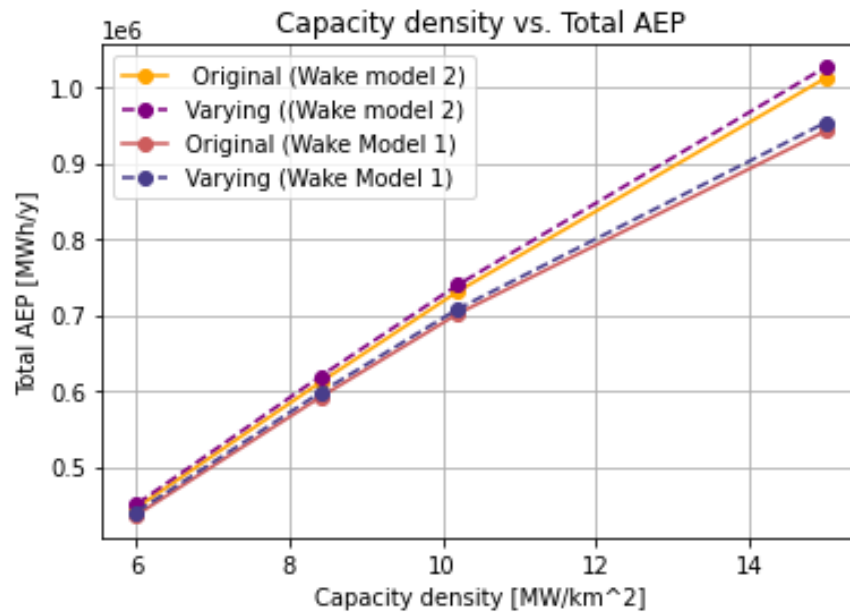


Figure 6.11: The total AEP [MWh/y] at different capacity densities for Project Case 2. Both Wake Models 1 and 2 are included in the figure.

### Capacity factor evaluation

The capacity factors for Project Case 2 are plotted versus capacity density in Figure 6.12. The figure includes both original and varying hub height scenarios, and concerns wind farms with capacity densities between 6-15  $MW/km^2$ . Both Wake Models 1 and 2 are also included. The capacity factor decreases continuously as the capacity density increases for all the implemented scenarios. By analysis with Wake Model 1, the capacity factors increased by 0.28-0.34 % for all capacity densities by varying the turbine hub heights, with the more significant increase for the wind farm with a capacity density of 15  $MW/km^2$ . For the Wake model 2 scenarios, the capacity factor increases by 0.37-0.44 % due to hub height variation for all capacity densities.

The figure indicates significantly higher capacity factors with Wake Model 2 than Wake Model 1 in Project Case 2, and the difference between the models increases as the capacity density increases. After a capacity density of 10  $MW/km^2$ , the capacity factors decrease for both original and varying hub height. However, the decrease is more drastic for the Wake Model 1 case than for the Wake Model 2 case. For all capacity densities, the impact of the 3D micro-siting is considerably greater for the Wake Model 2 case than for the Wake Model 1 case.

According to the capacity factor for the Wake Model 1 scenario, the capacity density can be increased from approximately 6-7  $MW/km^2$  by implementing the 3D micro-siting approach. An increase in capacity density includes a reduction of the distance between the turbines, which in this case consists of a decrease of 150 m. In this case, the capacity factor can stay the same with a simultaneous increase in AEP. For Wake Model 2, the capacity density can increase from 6  $MW/km^2$  to approximately 7.5  $MW/km^2$  in the same case, including a 200 m reduction in turbine spacing. This change can considerably affect a wind farm's energy production and capacity factor.



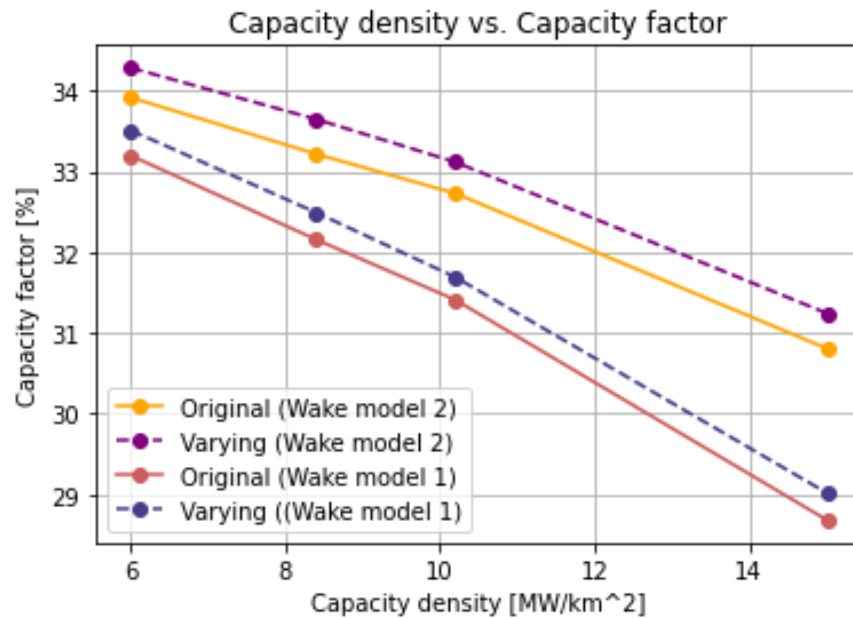


Figure 6.12: The capacity factor [%] at different capacity densities for Project Case 2. Both Wake Model 1 and 2 are included in the figure.

### Wake loss evaluation

Figure 6.13 compares the wake loss for the original and varying hub height wind farms in Project Case 2 for capacity densities between 6-15  $MW/km^2$ . Both Wake Models 1 and 2 are included in the figure. The figure shows that the wake loss increases evenly as the capacity density increases for both wake scenarios with original and varying turbine hub heights. Analysis with Wake Model 1 indicates a wake loss decrease of 0.2-0.32 % by varying the turbine hub heights, with the biggest decrease by the wind farm with the highest capacity density: 15  $MW/km^2$ . For the Wake Model 2 scenario, the wake loss decreases by 0.33-0.53 % by hub height variation for capacity densities between 6-10.2  $MW/km^2$ . For higher capacity densities such as 15  $MW/km^2$ , the wake loss decreases by 0.79 % by implementing the approach. These results indicate an increasing benefit of the 3D micro-siting approach with increasing capacity density.

The wake losses for Project Case 2 are substantially higher with Wake Model 1 than Wake Model 2, and the difference grows as the capacity density increases. The wake loss with Wake Model 1 increases from around 6 % to approximately 18 % for the implemented capacity densities. For Wake Model 2, this case concerns a wake loss increase from under 4 % to approximately 12 %. The figure indicates that the impact of the hub height variation is more significant for the Wake Model 2 scenarios than for the Wake Model 1 scenarios, meaning that the wake loss decreases more with Wake Model 2 by performing the 3D micro-siting approach. The wake loss for both scenarios with Wake Model 1 also increases slightly faster as the capacity density increases compared to the Wake Model 2 scenarios.

The wake loss change due to hub height variation is small in this project case. As previously discussed, an increase in capacity density, including hub height variation, would not lead to a significant increase in wake loss, especially with Wake Model 1 implemented. With Wake Model 2, the increase in wake loss is more

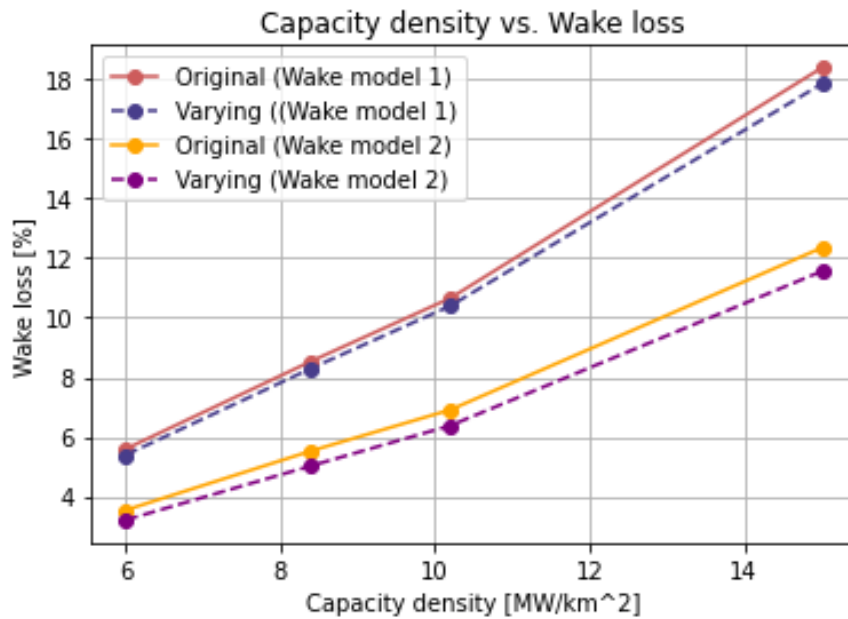


Figure 6.13: The wake loss [%] at different capacity densities for Project Case 2. Both Wake Models 1 and 2 are included in the figure.

considerable than for the Wake Model 1 scenarios by hub height variation. In a potential capacity density increase of a wind farm, both capacity factors and wake losses should be considered. For this increase, a compromise of the two parameters may be necessary. The AEP will increase with an increase in capacity density.

## 6.5 Results evaluation

By comparing the two main project cases in this study, the results show that the capacity factors in Project Case 2 are significantly lower than in Project Case 1. Both project cases include the 15 MW turbine, meaning the difference between them is the implemented wind regimes. For that reason, the lower capacity factors in Project Case 2 come from considerably lower wind speeds in its wind data. Despite the difference in capacity factor, the increase caused by hub height variation is approximately the same in both project cases for the lower capacity densities. However, for higher capacity densities, the increase in capacity factor is more pronounced for Project Case 1, which includes the high wind speed regime.

Project Case 1 in this study includes two parts with two different turbines implemented. Even though some capacity densities are the same, the results have clear differences. The wind farm capacity factors are higher for the wind farms with 15 MW turbines than the wind farms with 5 MW turbines. For a 5.4 MW/km<sup>2</sup> wind farm with 15 MW turbines, original hub heights, and implementation of Wake Model 1, the capacity factor is equal to 59.39 %. In the same case with 5 MW turbines, the capacity factor is equal to 56.47 %. There is a 3 % difference in capacity factor between the same capacity density with dissimilar turbines. The reason for this can be the significant difference in the number of turbines in the two cases since the wind farms with the 5 MW turbine need more turbines to achieve the same capacity density as with the 15 MW turbine. Simultaneously, this can also be a part of why the 3D micro-siting approach has more impact on

the wind farms with the 5 MW turbine, including more significant changes in the wake loss and capacity factor.

The results from the simulation with Wake Model 2 implemented for wake simulation showed that the total AEP and capacity factors were generally higher than with the implementation of Wake Model 1, including lower wake loss. By implementing the Wake Model 2, the impact of hub height variation was also more significant. Implementing Wake Model 2 to this three-dimensional micro-siting approach gave more considerable results according to the study's objective to minimise wake losses and maximise AEP. This finding can be due to the simplicity of Wake Model 1, and weakness in near-wake regions.

## 6.6 Uncertainties

There are several uncertainties in this kind of study, including simulation and testing. One uncertainty is that the wind farm layouts are not optimised. This means that the turbines' placement is not necessarily the best to gather the highest AEP and lowest wake losses. This study is performed within a time-limited period. Wind farm layout optimisation would have required more time and work to create an algorithm for the best layout. The wind farm layouts are designed with the same starting point: the power density at the site. However, as turbines were added, the layouts for each capacity density became quite different, considering the layout pattern. This difference can impact the variation in AEP and wake loss by varying hub heights. The comparison between original and varying hub height layouts can differ between the capacity densities.

Similarly, the wake models employed in the simulations are not tailored to the specific wind farms and wind conditions at the site, further adding to the uncertainties. The wake models used in this thesis are pre-implemented in WindSim and are quite simple and general for different wind farms with different wind conditions. Therefore, an optimisation of the wake models, including an increased complexity to the wake modelling, is necessary to fit the specific wind conditions. Non-optimised wake models can lead to inaccurate energy production and wake loss calculations, giving uncertainties to the results. High-fidelity wake models, such as CFD models like PyWakeEllipSys, can be relevant to the proposed approach. With this kind of wake model, a wider insight into the propagation of wake in wind farms can be gathered.

There are also uncertainties regarding the software's use and setup in WindSim. The simulation setup attempts to be as realistic as possible for an offshore wind farm, with the terrain, wind fields, etc. The chosen area represents the wind site well, but parameters like wave heights should be added, which was challenging to implement. The WindSim software is also still developing, which means that all effects (which create energy losses) that provide realism to the simulation could not be implemented.



## Chapter 7

# Conclusions

This thesis concerns a three-dimensional micro-siting approach of offshore wind farms at the auctioned wind site for wind energy utilisation at Southern Northsea II. The study implements two sets of wind data to test the approach in different wind conditions with different wind speeds. The first data set includes wind data from Southern Northsea II, with a high wind speed regime and a mean wind speed of 10.4 m/s. The second is from the Smøla wind site, with a moderate wind speed regime and a mean wind speed of 7.7 m/s. Two wind turbines with 5 MW and 15 MW installed capacity and two wake models, the Jensen and Larsen wake models, were implemented to perform the simulations. The simulations are performed using the CFD-based software WindSim.

While addressing the research question, the following conclusions are derived under this study:

**RQ1:** How can the wake loss be minimised and annual energy production (AEP) be maximised by applying the three-dimensional micro-siting in high and moderate wind speed regimes?

The wind farms with the high wind speed regime gather severely lower wake losses and higher AEP than the wind farms with moderate wind speed regimes. By varying the turbine hub heights in the wind farms, the wake loss will decrease, and the AEP will increase in both wind regimes. This improvement in AEP is due to the reduction in wake losses caused by the variable hub height installation of the wind turbines. The reduction in the wake losses and improvement in AEP are more prominent in higher capacity densities.

**RQ2:** How do the wind farm's capacity density and the turbine's rated capacity affect the wake losses and AEP in a three-dimensional micro-siting approach?

In this study, the original wind farms with 15 MW turbines have lower wake loss and higher AEP than the original wind farms with the 5 MW turbines. Nevertheless, it is seen that the proposed 3D micro-siting is more beneficial for the 5 MW turbine. Analysis of the wake loss in the 15 MW turbine wind farms indicates no significant change with 3D micro-siting for the lower capacity densities. The impact did increase as the capacity increased in simulation with both turbines. The wake loss and AEP in the study indicate the three-dimensional micro-siting approach is more beneficial as the capacity density of a wind farm increases.

In other words, with the three-dimensional micro-siting approach, the capacity density of wind farms could be increased without a substantial increase in the wake losses. Thus, with 3D micro-siting, the turbine spacing can be reduced, thereby increasing the possible nameplate capacity in a given area of a prospective wind farm.

**RQ3:** How would the above analysis on three-dimensional micro-siting be affected by the model chosen for the wake estimation?

By analysis of the different wake models, results indicated that the Larsen wake model generally gathered higher capacity factors and lower wake losses than the Jensen wake model in the two-dimensional and three-dimensional micro-siting. As the capacity density increased, the difference between the estimated values for the two wake models increased. The analysis also indicated that the cases with the Larsen wake model were more affected by a three-dimensional micro-siting than the opponent wake model, as the wake losses decreased and capacity factors increased by a more considerable amount.

According to the simulation results in this thesis, it is reasonable to consider moving the turbines in wind farms closer to each other and increasing their capacity density by implementing a three-dimensional micro-siting approach, including turbine hub height variation. By performing this method, the capacity factor and wake losses could stay the same, but the annual energy production of a wind farm will increase. This way, one can exploit the available offshore wind sites more efficiently. However, the micro-siting approach, wind farm layouts, and wake models must be optimised to exploit the areas as best as possible.

## 7.1 Further Research

Several points are worth considering in further research on the three-dimensional micro-siting topic of this thesis. These points include optimising the wind farm layouts and the implemented wake models. An optimisation of the layout would include using algorithms and different tools to gather the optimal placement of the turbines in a wind farm, which leads to an optimal wind farm layout. The fit of wake models will vary because of different wind conditions at different sites, and the precision of the models change compliantly. It would also be relevant to use high-fidelity wake models, for instance, CFD wake models such as PyWakeEllipSys, which can give more insights into the wake propagation pattern within the wind farm.

Since this thesis includes the micro-siting of offshore wind farms, other considerations should be included compared to onshore wind farms. In simulations of offshore wind farms, significant wave heights at the site and motion in the turbines should be included to create more realistic simulations. These properties could not be implemented in the simulations in this thesis. The actuator discs (AD) function in WindSim could have been used, but AD implementation would go at the expense of increased computational time and resources. This also concerns implementing the blockage effect using ADs, which was not completely developed in the used software and was not a priority in this time-limited process.



# References

- [1] E. G. Power. “All the benefits of wind power.” (), [Online]. Available: <https://www.enelgreenpower.com/learning-hub/renewable-energies/wind-energy/advantages-wind-energy>. (accessed: 15.01.2024).
- [2] nationalgrid. “Onshore vs offshore wind energy: What’s the difference?” (), [Online]. Available: <https://www.nationalgrid.com/stories/energy-explained/onshore-vs-offshore-wind-energy>. (accessed: 15.01.2024).
- [3] J. Lee and F. Zhao, “GWEC Global Wind Report 2024,” 2024, p. 148. [Online]. Available: <https://gwec.net/global-wind-report-2024/>.
- [4] The Norwegian Water Resources and Energy Directorate. “Identifisering av utredningsområder for havvind-sammendrag del 2.” (), [Online]. Available: <https://veiledere.nve.no/havvind/identifisering-av-utredningsomrader-for-havvind/sammendrag/sammendrag-del-1/>. (accessed: 16.01.2024).
- [5] The Norwegian Water Resources and Energy Directorate. “Image of the 20 new offshore areas.” (2024), [Online]. Available: <https://veiledere.nve.no/havvind/identifisering-av-utredningsomrader-for-havvind/kart/kart-brukt-i-leveransen/>.
- [6] The Norwegian Water Resources and Energy Directorate. “Identifisering av utredningsområder for havvind.” (2023), [Online]. Available: <https://veiledere.nve.no/havvind/identifisering-av-utredningsomrader-for-havvind/>.
- [7] J. Feng and W. Z. Shen, “Design optimization of offshore wind farms with multiple types of wind turbines,” vol. 205, pp. 1283–1297, 2017. DOI: <https://doi.org/10.1016/j.apenergy.2017.08.107>.
- [8] R. Shakoor, M. Hassan, A. Raheem, and Y.-K. Wu, “Wake effect modeling: A review of wind farm layout optimization using Jensens model,” vol. 58, pp. 1048–1059, 2016. DOI: <https://doi.org/10.1016/j.rser.2015.12.229>.
- [9] WindSim. “Wind resources.” (), [Online]. Available: <https://windsim.com/library/Module%20Overview/WindSim%20-%20Wind%20Resources.html>. (accessed: 11.01.2024).
- [10] J. Y. Jin, R. Ghani, and M. S. Virk, “Wind Turbine Wake Effects on Wind Resources Assessments-a Case Study,” vol. 186, no. 03003, pp. 1187–1207, 2020. DOI: <https://doi.org/10.1051/e3sconf/202018603003>.
- [11] S. Sharaf. “Offshore Wind Wake Effects Are Real: We Should Plan for Them.” Synapse Energy Economics. (), [Online]. Available: <https://www.synapse-energy.com/offshore-wind-wake-effects-are-real-we-should-plan-them>. 11.05.24.



- [12] C. L. Archer, A. Vassel-Be-Hagh, C. Yan, *et al.*, “Review and evaluation of wake loss models for wind energy applications,” vol. 226, pp. 1187–1207, 2018. DOI: <https://doi.org/10.1016/j.apenergy.2018.05.085>.
- [13] S. Brusca, R. Lanzafame, F. Famoso, *et al.*, “On the Wind Turbine Wake Mathematical Modelling,” *Energy Procedia*, vol. 148, pp. 202–209, 2018. DOI: <https://doi.org/10.1016/j.egypro.2018.08.069>.
- [14] M. Gu, Y. Wu, Y. Liu, and X. I. Yang, “A two-dimensional Jensen model with a Gaussian-shaped velocity deficit,” *Renewable Energy*, vol. 141, pp. 46–56, 2019. DOI: <https://doi.org/10.1016/j.renene.2019.03.127>.
- [15] M. Krutova and M. Bakhoday-Paskyabi, “Gaussian wake model fitting in a transient event over alpha ventus wind farm,” 2023. DOI: <https://doi.org/10.5194/wes-2023-79>.
- [16] M. Krutova, M. B. Paskyabi, F. G. Nielsen, and J. Reuder, “Evaluation of gaussian wake models under different atmospheric stability conditions: Comparison with large eddy simulation results,” *Renewable Energy*, vol. 141, pp. 46–56, 2020. DOI: [10.1088/1742-6596/1669/1/012016](https://doi.org/10.1088/1742-6596/1669/1/012016).
- [17] G. C. Larsen, “A simple stationary semi-analytical wake model,” 2009, Risø National Laboratory for Sustainable energy, Technical University of Denmark. [Online]. Available: <https://orbit.dtu.dk/en/publications/a-simple-stationary-semi-analytical-wake-model>.
- [18] S. Andersen, J. Sørensen, S. Ivanell, and R. Mikkelsen, “Comparison of Engineering Wake Models with CFD Simulations,” *J.Phys.: Conf.Ser.* 524 012161, 2014. DOI: [doi:10.1088/1742-6596/524/1/012161](https://doi.org/10.1088/1742-6596/524/1/012161).
- [19] L. Li, Y. Cui, L. Yongqian, L. Gao, N. Wang, and H. Lei, “Comparison and validation of wake models based on field measurements with lidar,” 2016, 66 (6.)–66 (6.) DOI: [10.1049/cp.2016.0587](https://doi.org/10.1049/cp.2016.0587).
- [20] K. Yang, “Determining an Appropriate Parameter of Analytical Wake Models for Energy Capture and Layout Optimization on Wind Farms,” vol. 13, no. 3, 2020. DOI: <https://doi.org/10.3390/en13030739>.
- [21] J. Hazra, S. Mitra, S. Mathew, and F. Zaini, “3D layout optimization for large wind farms,” in *2015 IEEE Power Energy Society Innovative Smart Grid Technologies Conference (ISGT)*, 2015, pp. 1–5. DOI: [10.1109/ISGT.2015.7131819](https://doi.org/10.1109/ISGT.2015.7131819).
- [22] J. Feng and W. Z. Shen, “Design optimization of offshore wind farms with multiple types of wind turbines,” *Applied Energy*, vol. 205, pp. 1283–1297, 2017. DOI: <https://doi.org/10.1016/j.apenergy.2017.08.107>.
- [23] Y. Chen, H. Li, B. He, P. Wang, and K. Jin, “Multi-objective genetic algorithm based innovative wind farm layout optimization method,” *Energy Conversion and Management*, vol. 105, pp. 1318–1327, 2015. DOI: <https://doi.org/10.1016/j.enconman.2015.09.011>.
- [24] L. Parada, C. Herrera, P. Flores, and V. Parada, “A novel approach for wind farm micro-siting in complex terrain based on an improved genetic algorithm,” *Energy*, vol. 25, p. 123970, 2022. DOI: <https://doi.org/10.1016/j.energy.2022.123970>.

- [25] L. Parada, C. Herrera, P. Flores, and V. Parada, “Coupled On-Site Measurement/CFD Based Approach for Wind Resource Assessment and Wind Farm Micro-Siting Over Complex Terrain,” *Energy*, vol. 25, p. 123 970, 2022. DOI: [10.1088/1755-1315/455/1/012037](https://doi.org/10.1088/1755-1315/455/1/012037).
- [26] K. Mjøllhus, “Three-dimensional micro-siting of a wind farm - A CFD based analysis,” 2020. [Online]. Available: <https://uia.brage.unit.no/uia-xmlui/handle/11250/2679620>.
- [27] H. Sun and H. Yang, “Wind farm layout and hub height optimization with a novel wake model,” *Applied Energy*, vol. 348, p. 121 554, 2023. DOI: <https://doi.org/10.1016/j.apenergy.2023.121554>.
- [28] M. Song, K. Chen, and J. Wang, “A two-level approach for three-dimensional micro-siting optimization of large-scale wind farms,” *Energy*, vol. 190, pp. 116–340, 2020. DOI: <https://doi.org/10.1016/j.energy.2019.116340>.
- [29] K.-H. Chang, “Chapter 19 - Multiobjective Optimization and Advanced Topics,” *e-Design Computer-Aided Engineering Design*, pp. 1105–1173, 2015. DOI: <https://doi.org/10.1016/B978-0-12-382038-9.00019-3>.
- [30] C. Meissner, A. R. Gravdahl, and D. Weir, “CFD Validation-A Simple Approach,” Nov. 2011. [Online]. Available: <https://windsim.com/Windsimarchive/library%20--%20papers-presentations/CFD%20Validation%20E2%80%93%20A%20Simple%20Approach.pdf>.
- [31] N. Simisiroglou, C. Meissner, and A. R. Gravdahl, “CFD wake modelling for offshore wind farms,” Nov. 2017. [Online]. Available: [https://windsim.com/Windsimarchive/library%20--%20paperspresentations/2017\\_WindEurope\\_WindSim\\_Uppsala\\_University%20CFD%20wake%20modelling%20for%20offshore%20wind%20farms.pdf](https://windsim.com/Windsimarchive/library%20--%20paperspresentations/2017_WindEurope_WindSim_Uppsala_University%20CFD%20wake%20modelling%20for%20offshore%20wind%20farms.pdf).
- [32] B. Xu, J. Zhu, J. Wen, and S. Lin, “Optimization for Variable Height Wind Farm Layout Model,” 2021. [Online]. Available: [https://www.researchgate.net/publication/352510657\\_Optimization\\_for\\_Variable\\_Height\\_Wind\\_Farm\\_Layout\\_Model](https://www.researchgate.net/publication/352510657_Optimization_for_Variable_Height_Wind_Farm_Layout_Model).
- [33] R. Shakoor, M. Hassan, A. Raheem, and Y.-K. Wu, “Wake effect modeling: A review of wind farm layout optimization using Jensens model,” vol. 58, pp. 1048–1059, 2016. DOI: <https://doi.org/10.1016/j.rser.2015.12.229>.
- [34] T. Ishihara, A. Yamagushi, and Y. Fujino, “Development of a new wake model based on a wind tunnel experiment,” Jan. 2004. [Online]. Available: [https://www.researchgate.net/publication/229014372\\_Development\\_of\\_a\\_new\\_wake\\_model\\_based\\_on\\_a\\_wind\\_tunnel\\_experiment](https://www.researchgate.net/publication/229014372_Development_of_a_new_wake_model_based_on_a_wind_tunnel_experiment).
- [35] N. Charhouni, “Qualification of three analytical wake models,” CFM 2015. [Online]. Available: <https://hal.science/hal-03446091/document>.
- [36] D. Zhao, N. Han, E. Goh, J. Cater, and A. Reinecke, “Wind Turbines and Aerodynamics Energy Harvesters,” in Academic Press, 2019, ch. 7-Aerodynamics of horizontal axis wind turbines and wind farms, pp. 444–446. DOI: <https://doi.org/10.1016/C2018-0-01955-6>.
- [37] WindSim. “Wind Fields.” (), [Online]. Available: <https://windsim.com/library/Module%20Overview/WindSim%20-%20Wind%20Fields.html>. (accessed: 12.01.2024).
- [38] S. Mathew, *Wind Energy-Fundamentals, Resource Analysis and Economics*. Springer, 2006, pp. 29–32, ISBN: 3-540-30905-5.

- [39] P. G. Jamdade, S. V. Patil, and V. B. Patil, "Assessment of Power Coefficient of an Offline Wind Turbine Generator System," *International Journal of Engineering Research Technology (IJERT)*, vol. 2, p. 2, 2013. [Online]. Available: <https://www.ijert.org/research/assessment-of-power-coefficient-of-an-offline-wind-turbine-generator-system-IJERTV2IS90929.pdf>.
- [40] M. L. and J. Buhl, "A New Empirical Relationship between Thrust Coefficient and Induction Factor for the Turbulent Windmill State," *Technical Report NREL/TP-500-36834*, p. 2, 2005. [Online]. Available: <https://www.nrel.gov/docs/fy05osti/36834.pdf>.
- [41] J. Manwell, J. McGowan, and A. L. Rogers, *Wind Energy Explained- Theory, Design and Application- Chapter 3*. Wiley, 2009, pp. 83–105, ISBN: 978-0-470-01500-1. [Online]. Available: [https://ee.tlu.edu.vn/Portals/0/2018/NLG/Sach\\_Tieng\\_Anh.pdf](https://ee.tlu.edu.vn/Portals/0/2018/NLG/Sach_Tieng_Anh.pdf).
- [42] M. Blackwood, "Maximum Efficiency of a Wind Turbine," *Undergraduate Journal of Mathematical Modeling: One + Two*, vol. 6, no. 2, 2016. [Online]. Available: <https://digitalcommons.usf.edu/cgi/viewcontent.cgi?article=4865&context=ujmm>.
- [43] J. Manwell, J. McGowan, and A. L. Rogers, *Wind Energy Explained- Theory, Design and Application*. Wiley, 2009, pp. 30–40, ISBN: 978-0-470-01500-1. [Online]. Available: [https://ee.tlu.edu.vn/Portals/0/2018/NLG/Sach\\_Tieng\\_Anh.pdf](https://ee.tlu.edu.vn/Portals/0/2018/NLG/Sach_Tieng_Anh.pdf).
- [44] S. Mathew, *Wind Energy-Fundamentals, Resource Analysis and Economics*. Springer, 2006, p. 68, ISBN: 3-540-30905-5.
- [45] SIMSCALE. "K-Epsilon Turbulence Models." (), [Online]. Available: <https://www.simscale.com/docs/simulation-setup/global-settings/k-epsilon/>. (accessed: 18.04.2024).
- [46] E. Branlard, E. Quon, A. R. M. Forsting, J. King, and P. Moriarty, "Wind farm blockage effects: Comparison of different engineering models," *Journal of Physics: conference Series*, 2020. DOI: 10.1088/1742-6596/1618/6/062036.
- [47] N. Boccard, "Capacity Factor of Wind Power - Realized Values vs. Estimates," p. 1, 2008. [Online]. Available: <https://docs.wind-watch.org/Boccard-Capacity-Factor-Of-Wind.pdf>.
- [48] M. Blackwood, "Undergraduate Journal of Mathematical Modeling: One + Two: Vol. 6: Iss. 2, Article 2.," vol. 6, pp. 3–5, 2016. [Online]. Available: <https://digitalcommons.usf.edu/cgi/viewcontent.cgi?article=4865&context=ujmm>.
- [49] H. Shi, Z. Dong, N. Xiao, and Q. Huang. "Wind Speed Distributions Used in Wind Energy Assessment: A Review." (), [Online]. Available: <https://www.frontiersin.org/articles/10.3389/fenrg.2021.769920/full>. (accessed: 15.01.2024).
- [50] S. Mathew, *Wind Energy-Fundamentals, Resource Analysis and Economics*. Springer, 2006, pp. 75–76, ISBN: 3-540-30905-5.
- [51] W. A. with Dr. Catherine Meissner, "Windsim getting started," pp. 1–3, 2019. [Online]. Available: <https://windsim.com/Windsimarchive/Getting%20Started.pdf>.
- [52] T. Wallbank, "WindSim Validation Study," 2008. [Online]. Available: <https://windsim.com/Windsimarchive/library%20--%20papers-presentations/080512trw%20WindSim%20Write%20Up%20-%20Validation%20study.pdf>.

- [53] WindSim, “Getting Started WindSim 12,” pp. 1–3, 2023. [Online]. Available: <C:/Program%20Files/WindSim/WindSim%2012.0.0/Documentation/Getting%20Started.pdf>.
- [54] WindSim. “Terrain.” (), [Online]. Available: <https://windsim.com/library/Module%20overview/WindSim%20-%20Terrain.html>. (accessed: 11.01.2024).
- [55] WindSim. “Objects.” (), [Online]. Available: <https://windsim.com/library/Module%20overview/WindSim%20-%20Objects.html>. accessed: 11.01.2024.
- [56] WindSim. “Results.” (), [Online]. Available: <https://windsim.com/library/Module%20overview/WindSim%20-%20Results.html>. (accessed: 22.01.2024).
- [57] WindSim. “Energy.” (), [Online]. Available: <https://windsim.com/library/Module%20overview/WindSim%20-%20Energy.html>. (accessed: 15.01.2024).
- [58] National Renewable Energy Laboratory. “2019ORCost\_NREL\_Reference\_15MW\_248.” (2023), [Online]. Available: [https://nrel.github.io/turbine-models/2019ORCost\\_NREL\\_Reference\\_15MW\\_248.html](https://nrel.github.io/turbine-models/2019ORCost_NREL_Reference_15MW_248.html).
- [59] GitHub. “NREL Reference 15 MW Offshore Wind Turbine Cost Data.” (2020), [Online]. Available: [https://github.com/NREL/turbine-models/blob/master/Offshore/2019ORCost\\_NREL\\_Reference\\_15MW\\_248.csv](https://github.com/NREL/turbine-models/blob/master/Offshore/2019ORCost_NREL_Reference_15MW_248.csv).
- [60] K. Kleeberg, “Workshop: AD and Blockage Effect Module,” 2021. [Online]. Available: [https://windsim.com/wp-content/uploads/2021/03/2106\\_WindSim\\_UM\\_WS\\_Katja\\_Kleeberg%20-%20Workshop%20AD%20and%20Blockage%20Effect%20Module.pdf](https://windsim.com/wp-content/uploads/2021/03/2106_WindSim_UM_WS_Katja_Kleeberg%20-%20Workshop%20AD%20and%20Blockage%20Effect%20Module.pdf).
- [61] The Norwegian Water Resources and Energy Directorate. “Identifisering av utredningsområder for havvind-Sørvest F (inkludert Sørliche Nordsjø II).” (), [Online]. Available: <https://veiledere.nve.no/havvind/identifisering-av-utredningsomrader-for-havvind/nye-omrader-for-havvind/sorvest-f-inkl-sorlige-nordsjo-ii/>. (accessed: 16.04.2024).
- [62] J.Jonkman, S. Butterfield, W.Musial, and G.Scott, “Definition of a 5-MW Reference Wind Turbine for Offshore System Development,” p. 2, 2009. [Online]. Available: <https://www.nrel.gov/docs/fy09osti/38060.pdf>.

# Appendix A

## Project Case 1 with 5 MW turbines

### A.1 Wake Model 1 results

Tables A.1 and A.2 present the results from Project Case 1 with 5 MW turbines, with Wake Model 1. The tables present the results with original and varying hub heights, respectively, with capacity densities from 5.4-8  $MW/km^2$ .

Table A.1: Results for Project Case 1 wind farms with 5 MW turbines with original hub height, including Wake Model 1 for wake simulation.

Parameter	Capacity density [ $MW/km^2$ ]				
	5.4	6	6.4	7	8
Total installed capacity [kW]	135 000	150 000	160 000	175 000	200 000
Total AEP [MWh/y]	667789.9	736543.2	785021.5	853750.4	963962.5
Wake loss [%]	3.69	4.36	4.45	4.98	6.1
Capacity factor [%]	56.47	56.05	56.01	55.69	55.02

Table A.2: Results for Project Case 1 wind farms with 5 MW turbines with varying hub height, including Wake Model 1 for wake simulation.

Parameter	Capacity density [ $MW/km^2$ ]				
	5.4	6	6.4	7	8
Total installed capacity [kW]	135 000	150 000	160 000	175 000	200 000
Total AEP [MWh/y]	675533.5	747909.8	796707.2	866363.2	977951.9
Wake loss [%]	3.38	3.96	4.09	4.52	5.64
Capacity factor [%]	57.12	56.92	56.84	56.51	55.82

## A.2 Wake Model 2 results

Tables A.3 and A.4 present the original and varying hub height results for Project Case 1 with 5 MW turbines and Wake Model 2 included as wake simulation. The results include capacity densities between 5.4-8  $MW/km^2$ .

Table A.3: Results for Project Case 1 wind farms with 5 MW turbines with original hub height, including Wake Model 2 for wake simulation.

Parameter	Capacity density [ $MW/km^2$ ]				
	5.4	6	6.4	7	8
Total installed capacity [kW]	135 000	150 000	160 000	175 000	200 000
Total AEP [MWh/y]	675683.5	747083	796189.3	867818.7	983782.4
Wake loss [%]	2.55	2.99	3.09	3.41	4.17
Capacity factor [%]	57.14	56.86	56.81	56.61	56.15

Table A.4: Results for Project Case 1 wind farms with 5 MW turbines with varying hub height, including Wake Model 2 for wake simulation.

Parameter	Capacity density [ $MW/km^2$ ]				
	5.4	6	6.4	7	8
Total installed capacity [kW]	135 000	150 000	160 000	175 000	200 000
Total AEP [MWh/y]	683549.9	758806.2	808563	880744.4	998554.6
Wake loss [%]	2.23	2.57	2.66	2.94	3.65
Capacity factor [%]	57.8	57.75	57.69	57.45	57

# Appendix B

## Project Case 1 with 15 MW turbines

### B.1 Wake Model 1 results

Tables B.1 and B.2 present the results for the Project Case 1 wind farms with the 15 MW turbine with original and varying hub heights. In this case, Wake Model 1 is used for the wake simulation. The tables include the total installed capacity, total AEP, wake loss and capacity factor for the wind farms with the capacity densities from 5.4-10.2  $MW/km^2$ .

Table B.1: Results for Project Case 1 wind farms with 15 MW turbines with original hub height, including Wake Model 1 for wake simulation.

Parameter \ Capacity density [ $MW/km^2$ ]	5.4	6.6	8.4	9.6	10.2
Total installed capacity [kW]	135 000	165 000	210 000	240 000	255 000
Total AEP [MWh/y]	702316.1	845217.8	1061571.2	1205018.2	1266115.9
Wake loss [%]	3.56	5.03	6.28	6.92	7.95
Capacity factor [%]	59.39	58.48	57.71	57.32	56.67

Table B.2: Results for Project Case 1 wind farms with 15 MW turbines with varying hub height, including Wake Model 1 for wake simulation.

Parameter	Capacity density [ $MW/km^2$ ]	5.4	6.6	8.4	9.6	10.2
	Total installed capacity [kW]		135 000	165 000	210 000	240 000
Total AEP [MWh/y]		705950.1	850459.7	1067198	1212029.1	1273884.4
Wake loss [%]		3.53	4.97	6.24	6.89	7.89
Capacity factor [%]		59.69	58.84	58.01	57.65	57.03

In addition to the mentioned capacity densities, wind farms with 12 and 15  $MW/km^2$  have been simulated to investigate when the wake losses increase and the capacity factor decreases drastically. The results from the 12 and 15  $MW/km^2$  wind farms are presented in Tables B.3 and B.4. The tables include the total installed capacity and AEP, wake loss and capacity factor for original and varying hub heights, and the case difference.

Table B.3: Results from the wind farm layout with 12  $MW/km^2$  and 15 MW turbines.

Parameter	Original hub height	Varying hub height	Difference
Total installed capacity [kW]	300000	300000	-
Total AEP with wake losses [MWh/y]	1441218.2	1451049.9	9831.7
Wake loss [%]	10.91	10.80	-0.11
Capacity factor [%]	54.84	55.21	0.3741

Table B.4: Results from the wind farm layout with 15  $MW/km^2$  and 15 MW turbines.

Parameter	Original hub height	Varying hub height	Difference
Total installed capacity [kW]	375000	375000	-
Total AEP with wake losses [MWh/y]	1746233	1760897.8	14664.8
Wake loss [%]	13.65	13.33	-0.32
Capacity factor [%]	53.16	53.60	0.44



## B.2 Wake Model 2 results

Tables B.5 and B.6 present the results from Project Case 1 with the 15 MW turbine for both original and varying turbine hub height. Larsen's wake model is used for the wake simulation for these results. The tables include the installed capacity, total AEP, wake loss and capacity factor for capacity densities between 5.4-10.2  $MW/km^2$ .

Table B.5: Results for Project Case 1 with Wake Model 2, including the 15 MW turbine with original hub height.

Capacity density [ $MW/km^2$ ]	5.4	6.6	8.4	9.6	10.2
Parameter					
Total installed capacity [kW]	135 000	165 000	210 000	240 000	255 000
Total AEP [MWh/y]	711548	861767.1	1086807.1	1294879.4	1294879.4
Wake loss [%]	2.3	3.18	4.05	4.43	5.85
Capacity factor [%]	60.17	59.62	59.09	58.85	57.97

Table B.6: Results for Project Case 1 with Wake Model 2, including the 15 MW turbine with varying hub height.

Capacity density [ $MW/km^2$ ]	5.4	6.6	8.4	9.6	10.2
Parameter					
Total installed capacity [kW]	135 000	165 000	210 000	240 000	255 000
Total AEP [MWh/y]	715462	867659.9	1093610.2	1246344.4	1304484.6
Wake loss [%]	2.23	3.05	3.92	4.26	5.59
Capacity factor [%]	60.5	60.03	59.45	59.28	58.4

Tables B.7 and B.8 present the results for the 12 and 15  $MW/km^2$  wind farms, including the 15 MW turbine with original and varying hub height. The tables include the total installed capacity, total AEP, wake loss, and capacity factor for the wind farms with original and varying, as well as the difference between them.

Table B.7: Results from the wind farm layout with 12  $MW/km^2$  and 15 MW turbines.

Parameter	Original hub height	Varying hub height	Difference
Total installed capacity [kW]	300000	300000	-
Total AEP with wake losses [MWh/y]	1501651.8	1515763.6	14111.8
Wake loss [%]	7.18	6.82	-0.36
Capacity factor [%]	57.14	57.68	0.54

Table B.8: Results from the wind farm layout with 15  $MW/km^2$  and 15 MW turbines.

Parameter	Original hub height	Varying hub height	Difference
Total installed capacity [kW]	375000	375000	-
Total AEP with wake losses [MWh/y]	1842050.2	1859934.9	17884.7
Wake loss [%]	8.92	8.45	-0.47
Capacity factor [%]	56.08	56.62	0.54

# Appendix C

## Project Case 2 with 15 MW turbines

### C.1 Wake model 1 results

Tables C.1 and C.2 present the results from Project Case 2 with Jensen’s wake model for the original hub height and varying hub height, respectively, for the different capacity densities. For both cases, the results include total AEP, wake loss and capacity factor for the capacity densities 6-15  $MW/km^2$ .

Table C.1: Results for the Project Case 2 wind farms with original hub heights and Jensen’s wake model included.

Capacity density [ $MW/km^2$ ]	6	8.4	10.2	15
Parameter				
Total installed capacity [kW]	150 000	210 000	255 000	375 000
Total AEP [MWh/y]	436205.4	591540.9	701617.5	942315.4
Wake loss [%]	5.59	8.54	10.66	13.65
Capacity factor [%]	33.2	32.16	31.41	28.69

Table C.2: Results for the Project Case 2 wind farms with varying hub heights and Jensen’s wake model included.

Capacity density [ $MW/km^2$ ]	6	8.4	10.2	15
Parameter				
Total installed capacity [kW]	150 000	210 000	255 000	375 000
Total AEP [MWh/y]	440316.8	597613.1	707974	953336.2
Wake loss [%]	5.39	8.3	10.40	13.33
Capacity factor [%]	33.51	32.49	31.69	29.02

## C.2 Wake model 2 results

The Project Case 2 results for the original and varying hub height, with Wake Model 2 as the wake simulation is presented in Tables C.3 and C.4. The tables contain the total installed capacity, AEP, wake loss and capacity factor for the capacity densities between 6-15  $MW/km^2$ .

Table C.3: The original hub height results for Project Case 2 with Wake Model 2.

Parameter	Capacity density [ $MW/km^2$ ]			
	6	8.4	10.2	15
Total installed capacity [kW]	150 000	210 000	255 000	375 000
Total AEP [MWh/y]	445644.4	611020.6	731052.2	1012040.9
Wake loss [%]	3.54	5.53	6.91	12.35
Capacity factor [%]	33.92	33.21	32.72	30.81

Table C.4: The varying hub height results for Project Case 2 with Wake Model 2.

Parameter	Capacity density [ $MW/km^2$ ]			
	6	8.4	10.2	15
Total installed capacity [kW]	150 000	210 000	255 000	375 000
Total AEP [MWh/y]	450472.8	618938.8	739723.6	1026357.4
Wake loss [%]	3.21	5.03	6.38	11.56
Capacity factor [%]	34.28	33.65	33.12	31.24